A Velocity Decomposition Approach for Unsteady Flow

by

Yang Chen

Advisor: Prof. Kevin J. Maki

A dissertation submitted in partial fulfillment
of the requirements for the degree of
Master of Science
(Naval Architecture and Marine Engineering)
in The University of Michigan
2014

ACKNOWLEDGEMENTS

I am very grateful to my advisor Dr. Kevin Maki, who led me in this amazing research. His constant encouragement and guidance have been extremely helpful. The previous work done by Bill Rosemurgy and Deborah Edmund is greatly appreciated. I am also thankful to Bill Rosemurgy for his helpful advice and the passionate discussion.

TABLE OF CONTENTS

LIST OF FIGURES

Figure

LIST OF TABLES

Table

CHAPTER I

Introduction

For many years, considerable work have been done by researches to gain better knowledge of the physics of fluid flow. Design and engineering application rely significantly on the understanding of the physics of the flow field in different design conditions. Nowadays, the main tools for analysis of fluid dynamics can be generally divided in to three different categories, theoretical, experimental and computational approaches. Even though a theoretical approach can provide a sophisticated point of view, such as the closed form mathematical expression of canonical problems, there is a gap between theoretical solutions and real life applications. Experiments, on the other hand, put us in intimate contact with all the physics involved in the problem and offers a direct interaction between the design and analysis. However, its applicability is tempered by the cost and challenges in creating the environment. Also, for engineering applications like naval engineering, it is not realistic to build a ship to test, especially in the early stage of design. With the rapid development of computational power, simulation of the flow field of the design using a digital computer has become a more and more important tool for designs and engineering applications. Significant effort has been put forth to make numerical simulation more applicable in the early design stage of all the engineering applications. Oracle team USA, the champion of the 2013 American cup (a world famous sailing competition) has claimed

that almost all of their design verification effort has relied substantially on numerical simulations.

There are various methods to perform numerical fluid flow simulations, such as potential flow based method, numerically solving the Navier-Stokes equations, and more exotic particle based methods, like Lattice-Boltzmann method. Due to its relative short development history and other limitations, particle based methods are still relatively restrictive in engineering applications, while the other two methods are widely applied based on different level of desired accuracy of approximation. When the viscous effects, such as boundary layer, separation and wake, can be ignored, the potential based methods are normally applied, because of its exceptional computation efficiency. The potential flow methods are widely used for preliminary designs. Especially in naval applications, potential flow methods are extensively exploited to calculate ship waves and predict wave-making resistance of the vessels. When the non-breaking wave is assumed and the flow at free-surface can be treated as irrotational, the potential flow methods can provide fairly accurate prediction for the waves generated by surface vessels. However, the potential flow methods are greatly limited by its irrotational assumption. When the viscous effects are important, then the viscous flow methods, numerically solving the Navier-Stokes equations, must be applied to capture the effects of viscosity. Even though viscous flow methods (or commonly called CFD) are more accurate and applicable in engineering application, they suffer from the relatively high computational cost. Hence, it is with appreciable benefits to combine the computation efficiency of potential methods and the accuracy of viscous flow methods. Considerable amount of effort has been spent for this goal in the literature.

1.1 Background

A straightforward utilization of the benefits of the potential flow solution to improve the accuracy and efficiency of the CFD solver is sometimes referred to as the "far-field correction", which is to set the potential velocity as the boundary condition of the CFD solver instead of using the free-stream velocity. In *Eça and Hoekstra* (2009), improvements of the Navier-Stokes solution is shown within a smaller domain through using this approach. However, the improvement is limited since the interaction between the viscous and inviscid solution has not been exploited. Since the viscous effects are usually confined within a small area around the body for most of the engineering applications, domain decomposition method is introduced to decomposed the flow domain into different regions and apply the suitable solution technique for each specific region. In *Campana et al.* (1995), the computational domain is decomposed into two parts, one contains the body and wake, the other one is the rest of the area. The conventional RANS method is applied to the former region which dominated by the viscous effects. Then the flow field at the other region is described by a potential model. These two domains are coupled by enforcing a matching condition within their overlap section. The domain decomposition approach in *Campana et al.* (1995) is carried further to solve for unsteady wave-breaking flows in *Iafrati and Campana* (2003). The fluid domain away from the free-surface is modeled using potential flow method. The fluid near the free-surface is solved using the RANS equation while the air-water interface is captured by a level-set technique.

Besides of the domain decomposition approach, the velocity vector can be generally decomposed into two parts, Then each component can be solved through its more suitable and sufficient method. This method is usually referred to as the velocity decomposition method. *Hafez et al.* (2006) and *Hafez et al.* (2007) exploited a Helmholtz velocity decomposition to decompose the velocity vector into a gradient

of potential and rotational component (a correction).

$$\boldsymbol{u} = \nabla\Phi + \boldsymbol{w} \tag{1.1}$$

Then the potential is solved through a Poisson equation with a source term due to the rotational velocity component. And the rotational component is obtained by solving the Naiver-Stokes equation through a conventional finite volume approach. A modified Bernoulli's law is implemented to generate pressure and couple the inviscid and viscous solutions. Since the potential is solved in the whole domain and coupled with the rotational component, some of the interface difficulties of the domain decomposition approach can be eliminated.

Kim et al. (2005) also applied the Helmholtz decomposition to derive a complementary RANS equations. Even though the same accuracy of the conventional RANS method is achieved through solving the complementary RANS equations, the improvement of computational efficiency is limited. *Kim et al.* (2005) noted that a different choice of the potential can lead to a faster converged solution and a smaller computational domain, which may result in further reduce of the computational time. Following the work of *Kim et al.* (2005), *Edmund et al.* (2011) applied the transpiration velocity, which is first introduced by *Lighthill* (1958), to the boundary condition. Some improvements of the solution were found when solving the flow problem on a reduced computational domain. *Morino* (1986) extensively discussed the use of the Helmholtz decomposition theorem in fluid dynamics. Relating the Helmholtz decomposition and the equivalent source approach (also known as transpiration-velocity approach), introduced by *Lighthill* (1958), *Morino* (1986) gave a generalized expression of this transpiration approach. Inspired by *Morino* (1986), *Edmund* (2012) (*Edmund et al.* (2013)) exploited the generalized expression of the transpiration-velocity approach. The vortical component is set to zero outside the viscous layer. Then the

potential velocity (referred to as viscous potential) satisfies the Navier-Stokes equation outside the vortical region and can be used as the correct boundary conditions on a reduced domain. A two way couple procedure is used to couple the vortical and irrotational components. Good agreement with the results generated by the conventional RANS approach was shown in steady two-, three-dimensional laminar and turbulent flows. A significant improvement in computation efficiency is shown. Based on the work by *Edmund* (2012), *Rosemurgy* (2014) (*Rosemurgy et al.* (2013), *Rosemurgy et al.* (2012), *Rosemurgy et al.* (2011)) extended the solver to be able to solve for steady lifting and free-surface flows. In this work, the velocity decomposition solver developed by *Edmund* (2012) and *Rosemurgy* (2014) is extended to be able to solve for unsteady flow.

1.2 Objectives

The objectives of this work is to demonstrate the ability of the velocity decomposition solver, developed by *Edmund* (2012) and *Rosemurgy* (2014), to solve unsteady flow problems. Promising results for steady flow problems have been shown by *Edmund* (2012) and *Rosemurgy* (2014). Additional procedures need to be established to applied the velocity decomposition method to generate time accurate solutions for unsteady flow problems. In this work, two approaches to calculate the unsteady viscous potential are proposed to improved computation efficiency.

The mathematical formulations, including the governing equations, boundary and initial conditions, of the conventional Navier-Stokes problem as well as the two velocity decomposition sub-problems, are described in chapter II. In chapter III, numerical implementations of the CFD solver, the velocity decomposition solver and the two approaches to calculate the viscous potential are discussed. Chapter IV presents the results of two-dimensional laminar flow over a flat plate with finite length and a cylinder. Conclusion and future work are discussed in chapter V.

CHAPTER II

Mathematical Formulation

This thesis is focused on applying velocity decomposition method to unsteady flow problem. In this Chapter the general mathematical formulations of the problems are stated. The governing equations, initial and boundary conditions for the conventional Navier-Stokes problems are described. The formulation of two sub-problems, which are generated after the velocity decomposition is applied, are expressed. Then, the viscous boundary condition required to solve for the viscous potential velocity in velocity decomposition is discussed in detail.

2.1 Conventional Navier-Stokes Problem

In this work, the flow problem, which is to directly solve the Navier-Stokes equations in a computational domain with appropriate initial and boundary conditions, is denoted as the Navier-Stokes problem. The flow domain is assumed infinite and two-dimensional in this work. The flow domain and boundaries are shown in figure 2.1, where $\partial\Omega_\infty$ denotes the boundary of the infinite flow domain which is far away from the body, $\partial\Omega_B$ is the body boundary and $\partial\Omega_R$ is the boundary of the reduced domain.

The whole problem is governed by the incompressible version of the Navier-Stokes equations and the continuity equation, shown in Eq.(2.1) and Eq.(2.2), which are

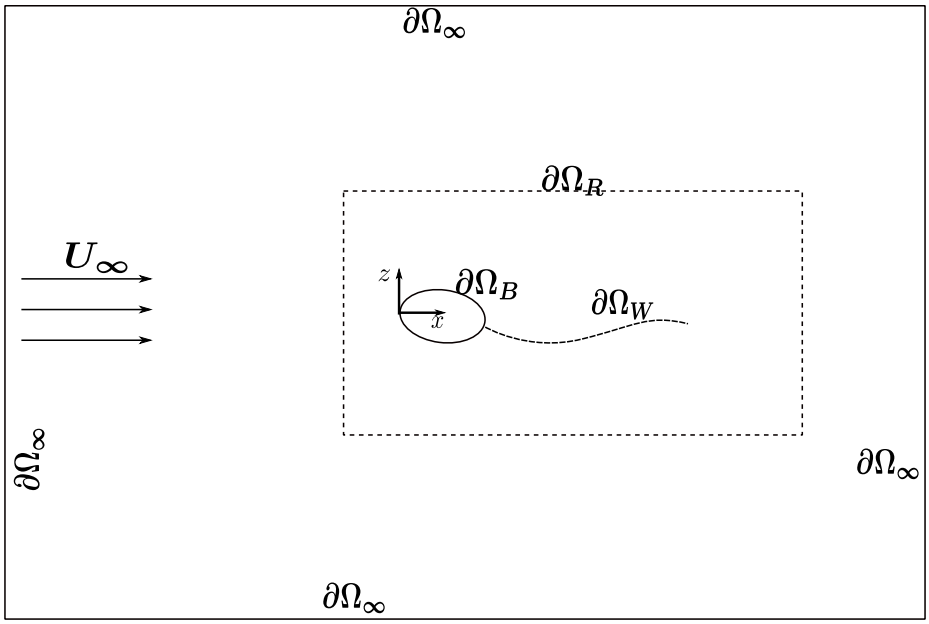

Figure 2.1: Definition of a general flow domain for the Navier-Stokes problem ($\partial\Omega_B$ is the body surface, $\partial\Omega_W$ is the wake surface, $\partial\Omega_R$ is the boundary of reduced domain)

derived from conservation of mass and momentum with the assumptions of constant viscosity and density.

$$\nabla \cdot \boldsymbol{u} = 0 \tag{2.1}$$

$$\frac{\partial \boldsymbol{u}}{\partial t} + \nabla \cdot (\boldsymbol{u}\boldsymbol{u}) = -\frac{\nabla p}{\rho} + \nabla \cdot \nu(\nabla \boldsymbol{u} + \nabla \boldsymbol{u}^T) \tag{2.2}$$

where $\boldsymbol{u} = \boldsymbol{u}(\boldsymbol{x}, t)$ is the total velocity field that varies in space and time, $\boldsymbol{u}\boldsymbol{u}$ in the second term means the tensor product, p is the dynamic pressure, ρ is the density of the fluid and ν is the kinematic viscosity, $()^T$ is the transpose. The dynamic pressure p is defined as total pressure P minus the static pressure, $p = P - \rho \boldsymbol{g} \cdot \boldsymbol{x}$, where $\boldsymbol{g}$ is the gravitational acceleration and $\boldsymbol{x}$ is the position vector. In this work, $\boldsymbol{g} = 0$, since buoyancy is not important for the cases studied.

2.1.1 Boundary and Initial Conditions

The velocity of viscous fluid on body is subject to the no-slip boundary condition which requires the fluid velocity to be equal to the velocity of the body, as shown in Eq.(2.3). Since only the flow problems with fixed bodies are considered in this work, the body boundary condition can be written as (2.4), in a body fixed coordinate.

$$\boldsymbol{u} = \boldsymbol{u}_B \qquad \text{on } \partial\Omega_B \tag{2.3}$$

$$\boldsymbol{u} = 0 \tag{2.4}$$

where $\boldsymbol{u}_B$ is the velocity of the body.

Meanwhile, the fluid velocity must satisfy the radiation condition, Eq.(2.5), which means the fluid velocity recovers the free-stream value far away from the body.

$$\lim_{|\boldsymbol{x}|\to\infty} \boldsymbol{u} = U_\infty \hat{i} \tag{2.5}$$

The initial velocity field of the domain excluding boundaries is prescribed by the initial condition, Eq.(2.6).

$$\boldsymbol{u}(\boldsymbol{x}, t)|_{t=0} = \boldsymbol{u}(\boldsymbol{x}, 0) = \boldsymbol{u}_0(\boldsymbol{x}) \tag{2.6}$$

where $\boldsymbol{u}_0$ is the initial velocity field.

Even though there are some widely used formations of pressure boundary conditions, the correct ones are still subjected to discussion and debate in the literature (*Rempfer* (2006)). Hence, the pressure boundary conditions applied in this work are discussed in chapter III, as they are parts of the numerical approach for solving the Navier-Stokes problem.

2.2 Velocity Decomposition

Following the formulation expressed in *Edmund* (2012) and *Rosemurgy* (2014), the velocity decomposition method utilizes the Helmholtz decomposition to represent the total flow velocity field $\boldsymbol{u}$ as the sum of an irrotational component $\nabla\varphi$ and a vortical component, $\boldsymbol{w}$.

$$\boldsymbol{u}(\boldsymbol{x},t) = \nabla\varphi(\boldsymbol{x},t) + \boldsymbol{w}(\boldsymbol{x},\boldsymbol{t}) \tag{2.7}$$

Hence, the original Navier-Stokes problem is decomposed into two sub-problem, one is a Navier-Stokes initial-boundary value problem in the reduced domain and the other is a viscous potential sub-problem in the whole domain. To better utilize this decomposition, the vortical component, $\boldsymbol{w}$, is set to zero outside the vortical region. Then the irrotational part of the velocity matches the real fluid velocity when the fluid is irrotational. The Navier-Stokes sub-problem is similar to the original problem except the total velocity is solved in a reduced domain with different boundary conditions. The viscous potential sub-problem is governed by the Laplace equation like conventional potential flow problems and solved via boundary integral method. However, to account for the viscous effect and to couple with the total velocity inside vortical region, new boundary conditions need to be developed.

2.2.1 Navier-Stokes Sub-problem

This sub-problem is essentially similar to the original Navier-Stokes problem except that it is defined inside a reduced domain with boundary $\partial\Omega_R$, as can be seen in Figure 2.1. The domain boundaries have changed from $\partial\Omega_\infty$ to the boundary of the reduced domain, Ω_R. So the boundary condition on $\partial\Omega_R$ has to be established. The boundary of the reduced domain is set to include the vortical region, which implies that the vortical component $\boldsymbol{w}$ is zero on $\partial\Omega_R$. So on $\partial\Omega_R$, a Dirichlet boundary

condition (Eq.(2.8)) can be stated as, the total velocity equals to the irrotational component, which can be determined from the viscous potential sub-problem.

$$\boldsymbol{u} = \nabla\varphi \qquad \text{on } \partial\Omega_R \tag{2.8}$$

Through Eq.(2.8), The Navier-Stokes sub-problem is coupled with the viscous potential sub-problem describe in section 2.2.2. The algorithm that used to couple the two sub-problems is discussed in chapter III. The governing equations, other boundary and initial conditions for this sub-problem stay the same as in Eq.(2.1)-(2.4), Eq.(2.6) of the original Navier-Stokes problem.

2.2.2 Viscous Potential Sub-problem

The velocity in the irrotational region in the flow field can be represented by the gradient of the viscous potential (Eq.(2.9)). Then the governing Laplace equation (Eq.(2.10)) can be derived by combining Eq.(2.9) and the continuity equation Eq.(2.1).

$$\boldsymbol{u}(\boldsymbol{x}, t) = \nabla\varphi(\boldsymbol{x}, t) \tag{2.9}$$

$$\nabla^2\varphi = 0 \tag{2.10}$$

It is worth knowing that the conventional potential flow problem is governed by the Laplace equation, Eq.(2.10) and usually solved with a Neumann condition, the non-penetration body boundary condition, Eq.(2.11).

$$\frac{\partial\varphi}{\partial n} = 0 \qquad \text{on } \partial\Omega_B \tag{2.11}$$

As discussed in *Chorin and Marsden* (1990), the solution for this Neumann problem, defined on a simply connected region, is unique. However, since the non-penetration

body boundary condition does not account for the viscous effects, the potential velocity calculated from the conventional potential flow problem does not represent the correct velocity even outside the vortical region. Hence, to generate the correct potential velocity (which is to change the solution of the original well-posed Neumann problem), either the governing equation or the boundary condition has to be changed. To include the viscous effects in the body boundary condition, a viscous body boundary condition is used to replace the non-penetration condition, Eq.(2.11). The solution corresponds to this viscous Neumann condition is designated as the viscous potential. Directly follow the derivation in *Edmund* (2012) and *Rosemurgy* (2014), the body boundary condition is stated as in Eq.(2.12)-(2.13). The Neumann body boundary condition Eq.(2.14) can derived as the inner product of Eq.(2.13) and the surface unit normal vector, $\hat{n}$.

$$\boldsymbol{u} = \nabla\varphi(\boldsymbol{x}, t) + \boldsymbol{w}(\boldsymbol{x}, t) = 0 \qquad \text{on } \partial\Omega_B \tag{2.12}$$

then

$$\nabla\varphi(\boldsymbol{x}, t) = -\boldsymbol{w}(\boldsymbol{x}, t) \qquad \text{on } \partial\Omega_B \tag{2.13}$$

$$\frac{\partial\varphi(\boldsymbol{x}, t)}{\partial n} = -\boldsymbol{w}(\boldsymbol{x}, t) \cdot \hat{n} \qquad \text{on } \partial\Omega_B \tag{2.14}$$

This new boundary condition, Eq.(2.14), implies that that the viscous potential velocity on the body is equal to the opposite of vortical component, which is essentially to alter the body shape according to viscous effect, such as boundary layer and viscous wake. So for the problems considered in this work, the viscous wake in downstream is also applied with this new boundary condition (Eq.(2.15)).

$$\frac{\partial\varphi(\boldsymbol{x}, t)}{\partial n} = -\boldsymbol{w}(\boldsymbol{x}, t) \cdot \hat{n} \qquad \text{on } \partial\Omega_W \tag{2.15}$$

Even though time variable is not explicitly present in the Laplace governing equa-

tion, both the viscous potential and the vortical velocity may be time dependent for unsteady flow. The unsteadiness can be implicitly included through the viscous boundary condition, Eq.(2.14). The time dependency in Eq.(2.14) may be due to the unsteadiness present in the boundary layer or wake of the flow. For different types of unsteadiness, it can be solved through specific approach relevant to its physics. Two different approaches are proposed in this work and discussed in chapter III.

Because the total velocity satisfies the continuity Eq.(2.1) and the irrotational part of the velocity is divergence-free, the vortical component of the velocity must also be divergence-free.

$$\nabla \cdot \boldsymbol{w} = 0 \tag{2.16}$$

Then Eq.(2.16) can be expressed in the local orthogonal coordinate system:

$$\frac{\partial w_t}{\partial t} + \frac{\partial w_n}{\partial n} = 0 \tag{2.17}$$

where the subscripts t, denotes the component of tangential direction, and subscript n is for the normal direction pointing out of the body.

Eq.(2.17) is then integrated along the normal direction out to a distance δ, Eq.(2.18). After rearranging, It can be simplified to equation Eq.(2.19).

$$\int_0^\delta \left(\frac{\partial w_t}{\partial t} + \frac{\partial w_n}{\partial n} \right) \mathrm{dn} = 0 \tag{2.18}$$

$$w_n(0) = \int_0^\delta \left(\frac{\partial w_t}{\partial t} \right) \mathrm{d}n + w_n(\delta) \tag{2.19}$$

If the upper limit of the integration, δ, is set large enough, which means it is far away from the body and lands outside the vortical region, where the vortical component of the velocity decomposition is zero. Then the Eq.(2.19) can be further simplified to

Eq.(2.20).

$$w_n(0) = \int_0^{\delta} \left(\frac{\partial w_t}{\partial t} \right) \mathrm{d}n \tag{2.20}$$

This can be substituted into Eq.(2.14), then the viscous Neumann boundary condition becomes Eq.(2.21).

$$\begin{aligned} \frac{\partial \varphi}{\partial n} &= -\boldsymbol{w} \cdot \hat{n} = w_n \\ &= -\int_0^{\delta} \left(\frac{\partial w_t}{\partial t} \right) \mathrm{d}n \qquad \text{on } \partial\Omega_B \text{ and } \partial\Omega_w \end{aligned} \tag{2.21}$$

In an infinite fluid domain, the velocity is also subjected to the radiation condition, Eq.(2.22), which means the disturbance due to the body decreases as the increase of the distance, $|\boldsymbol{x}|$, away from the body.

$$\lim_{|\boldsymbol{x}| \to \infty} (\nabla \varphi - \boldsymbol{U}_\infty) = 0 \tag{2.22}$$

This implies that the velocity of the flow field recovers the free-stream velocity far away from the body. This turns out is automatically satisfied by the fundamental solutions of the Laplace equation. Hence, the governing equation Eq.(2.10), radiation boundary condition Eq.(2.22) and the new Neumann body boundary condition Eq.(2.21) define the viscous potential sub-problem. The numerical implementation and the solution strategy of the two sub-problems are discussed in chapter III.

CHAPTER III

Numerical Implementation

The mathematical description of the problems are described in chapter II. The discretization and numerical solution techniques to solve for the problems need to be selected. In this chapter, the numerical solution methods and the implementation are discussed. First, the solution strategy for the Navier-Stokes initial boundary value problem is described. Then, the solution method for solving the viscous potential sub-problem is presented, followed by the discussion of the iteration algorithm of the unsteady velocity decomposition solver and the description of its parameters.

3.1 Navier-Stokes Solution Method

The continuum mechanics problems solver environment, OpenFOAM, is used to solve the Navier-Stokes problem, because of its vast open source libraries, including CFD solvers, discretization scheme and so on. For discretization of the Navier-Stokes equations, Eq.(3.2), Finite Volume method (FVM), which is the most commonly used method in CFD today, is used. The whole computational domain is discretized by structured mesh. The governing equations, Eq.(3.1)-(3.2), of the Navier-Stokes

problem are restated here for convenience.

$$\nabla \cdot \boldsymbol{u} = 0 \tag{3.1}$$

$$\frac{\partial \boldsymbol{u}}{\partial t} + \nabla \cdot (\boldsymbol{u}\boldsymbol{u}) = -\frac{\nabla p}{\rho} + \nabla \cdot \nu(\nabla \boldsymbol{u} + \nabla \boldsymbol{u}^T) \tag{3.2}$$

Eq.(3.1)-(3.2) are the differential forms of the conservation of mass and momentum for each fluid element. In finite volume approach, they need to be integrated over a control volume and in time to produce the integral form of the governing equations, Eq.(3.3)-(3.4).

$$\int_V \nabla \cdot \boldsymbol{u} \mathrm{dV} = \int_S \boldsymbol{u} \mathrm{d}\boldsymbol{A} = 0 \tag{3.3}$$

$$\int_t^{t+\Delta t} \left[\int_V \frac{d\boldsymbol{u}}{dt} + \nabla \cdot (\boldsymbol{u} \otimes \boldsymbol{u}) - \nabla \cdot \nu(\nabla \boldsymbol{u} + \nabla \boldsymbol{u}^T) \mathrm{d}V \right] \mathrm{d}t = -\int_t^{t+\Delta t} \int_V \frac{\nabla p}{\rho} \mathrm{dVdt} \tag{3.4}$$

Then they must be transformed through discretization schemes into a corresponding system of algebraic equations. The solutions of these algebraic equations correspond to the solutions of the original set of equation in certain time and space.

For the time derivative term, the implicit Euler differencing scheme is used for discretization. The gradient and Laplacian terms are integrated using Gaussian integration with linear interpolation of the cell center values to the face centers. The divergence terms are also calculated with Gaussian integration, but linear upwind interpolation is used instead.

After applying the discretization scheme described above, the PISO (Pressure Implicit with Splitting of Operators) procedure proposed by *Issa* (1986), is used to solve for the velocity and pressure. More detailed discussion about the discretization techniques and the numerical solution method of the Navier-Stokes equation can be found in *Ferziger and Perić* (1996). For conventional Navier-Stokes problem, the

pressure boundary conditions are commonly set as in Eq.(3.5) and Eq.(3.6).

$$p = 0 \qquad \text{on } \partial\Omega_O \tag{3.5}$$

$$\frac{\partial p}{\partial n} = 0 \qquad \text{on rest of the boundaries} \tag{3.6}$$

The pressure directly outside the reduced domain can be calculated through the viscous potential velocity using Bernoulli's law. Then the pressure gradient boundary conditions for the Navier-Stokes sub-problem can be calculated using a two point finite difference scheme, as described in *Rosemurgy* (2014).

3.2 Viscous Potential Solution Method

The solution methodology is very similar to the boundary element method, which is widely used for solving conventional potential flow problems. This method is extensively discussed in *Katz and Plotkin* (2001). In the viscous potential sub-problem, the general solution of the Laplace governing equation can be constructed by the sum of the fundamental solutions distributed on the boundary surface. The fundamental solutions can be generated by relating Green's second identities to the Laplace equation. Since only the flow problem with no circulation is considered in this work, the basic solution of a point source (Eq.(3.7)) is selected. Then the constant strength source distribution over the boundary surface can be formed as in Eq.(3.8). Because the focus of this work is to demonstrate the algorithm of velocity decomposition solver solving unsteady flow, only the constant source panel method is applied. However, it should be kept in mind that other more sophisticated methods can be readily applied. The constant source panel is coincided with the body discretization from the finite

volume method.

$$\phi = \frac{\sigma}{2\pi} \ln r \tag{3.7}$$

$$\phi = \frac{1}{2\pi} \int_{\partial\Omega_B + \partial\Omega_W} \sigma \ln r \mathrm{d}S \tag{3.8}$$

where σ is the strength of the point source. r is the distance from the point source.

It is important to include $\partial\Omega_W$ in the surface integral. The source distribution over the wake surface is able to account for the viscous effect in the wake after the body, such as separation. This is one of the advantages of velocity decomposition compared to conventional inviscid potential method. The radiation boundary condition Eq.(2.22) is automatically satisfied by the fundamental solution Eq.(3.7). To include the free-stream flow and have the source distributions act as the disturbance potential, ϕ, Eq.(3.8) is written as Eq.(3.9).

$$\begin{aligned} \varphi &= \phi + \Phi_\infty \\ &= \frac{1}{2\pi} \int_{\partial\Omega_B + \partial\Omega_W} \sigma \ln r \mathrm{d}S + \boldsymbol{U}_\infty \cdot \boldsymbol{x} \end{aligned} \tag{3.9}$$

where $\Phi_\infty = \boldsymbol{U}_\infty \cdot \boldsymbol{x}$ is the free-stream potential. Now the frame of the solution for viscous potential is formed (Eq.(3.9)). The strength, σ, of the source distribution must to be determined. This is solved by imposing the viscous Neumann boundary condition, Eq.(2.21). Then, the term contains free-stream potential can be move to right hand side since it is known. This results in Eq.(3.10).

$$\frac{\partial \phi}{\partial n} = -\boldsymbol{U}_\infty \cdot \hat{n} - \boldsymbol{w} \cdot \hat{n} \qquad \text{on } \partial\Omega_B \text{ and } \partial\Omega_W \tag{3.10}$$

The influence coefficient, the part of the integral that excludes the source strength, of the constant source distribution is analytically calculated using the expressing provided in *Katz and Plotkin* (2001). Eq.(3.11)and Eq.(3.12) represent the velocity,

expressed in Cartesian coordinates, at point p in space, due to a source panel.

$$u_p = \frac{\partial \phi}{\partial x_p} = \frac{\sigma}{4\phi} \ln \frac{(x - x_1)^2 + z^2}{(x - x_2)^2 + z^2} \tag{3.11}$$

$$w_p = \frac{\partial \phi}{\partial z_p} = \frac{\sigma}{2\phi} \left[\tan^{-1} \frac{z}{x - x_2} - \tan^{-1} \frac{z}{x - x_1} \right] \tag{3.12}$$

$$\tag{3.13}$$

where the subscript p represent the point in space, The subscripts 1 and 2 are denoted as the two end-points of a panel, as shown in Fig.3.1. After the potential velocity in

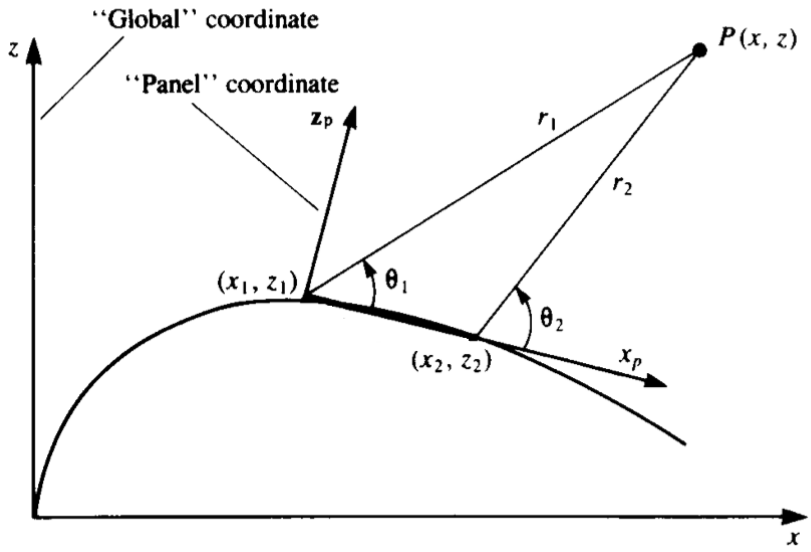

Figure 3.1: coordinate definition for the two-dimensional perturbation potential (*Katz and Plotkin* (2001))

point p is calculated in the panel coordinate, a rotation matrix is applied to transform it to the global coordinated. The potential velocity in each point is resulted by the sum of the influence of all the source panels. Combining all the influence of all the source panels and enforcing the viscous boundary condition, Eq.(3.10), at each panel on body and wake surface. This will result in a system of algebraic equations, Eq.(3.14)

$$[C]\,[\sigma] = -\,[\boldsymbol{U}_\infty \cdot \hat{n}] - [w_n] \qquad \text{on } \partial\Omega_B \text{ and } \partial\Omega_W \tag{3.14}$$

where $[C]$ is the matrix of influence coefficients. The system is solved by the open source linear algebra package, LAPACK. The matrix of influence coefficient is inverted by LU decomposition.

3.3 Unsteady Velocity Decomposition

One of the main advantages of velocity decomposition approach is to lower computational cost by considerably reducing the computational domain that CFD solver need to solve on. The methodology of the unsteady velocity decomposition solver is to generate a time-accurate viscous potential velocity and apply that to the inlet and far-field boundary of the reduced domain. To calculate the viscous potential velocity that can satisfy the Navier-Stokes equations directly outside the vortical region, the viscous boundary condition is required (Eq.(3.10)). Hence the vortical velocity need to be calculated. Since the vortical velocity, $\boldsymbol{w}$ is calculated as in Eq.(3.15), the vortical velocity is not known until the velocity field is calculated.

$$\boldsymbol{w} = \boldsymbol{u} - \nabla\varphi \tag{3.15}$$

So a iteration algorithm needs to be applied to solve for the vortical velocity. In this section, the algorithm of unsteady velocity decompositions solver is described. Then, two proposed methods for calculating the viscous potential are discussed. At the end of the section, the parameters governing the unsteady velocity decomposition solver are summarized.

3.3.1 Unsteady Velocity Decomposition Algorithm

The algorithm used by the unsteady velocity decomposition solver is shown in the form of a flowchart in Fig.3.2. Each step of the algorithm is described below:

1. Initialize the solver. If simulation start from $t = 0$, then go to step 2. If not,

go to step 3.

2. Apply the inviscid potential velocity, $\nabla\phi_{inv}$, as the boundary condition on the inlet and far-field boundary of the reduced domain.

3. Use CFD solver to solve for the Navier-Stokes sub-problem in the reduced domain with the new inlet and far-field boundary condition. If update conditions are reached, then go to step 4.

4. calculate the viscous potential.

5. Apply viscous potential velocity, $\nabla\varphi$, as the boundary condition on the inlet and far-field boundary of the reduced domain.

6. Repeat step 3 to step 5 until the number of updates specified by the user is reached.

7. When the time equals the end time, the solver is terminated.

In Fig.3.2, t_{end} is the end time of the simulation, t_{update} is the time to update, n_{update} and N_{update} is the update counter and the total number of updates respectively. The update in the algorithm means the process of applying the viscous potential velocity to the reduced domain boundary, $\partial\Omega_R$.

The methods and procedures presented so far are essentially similar to those in *Edmund* (2012) and *Rosemurgy* (2014). However, to solve the unsteady flow problems, more need to be done, since the velocity of the transient flow varies in time, which means both the viscous potential and the vortical velocity can be time dependent, as stated in Eq.(3.16).

$$\boldsymbol{u}(\boldsymbol{x},t) = \nabla\varphi(\boldsymbol{x},t) + \boldsymbol{w}(\boldsymbol{x},t) \tag{3.16}$$

Therefore, a new procedure need to established to solve for the unsteady viscous potential. In the following subsections, two approaches for calculating the unsteady

viscous potential are proposed to solve for different types of unsteadiness in the flow.

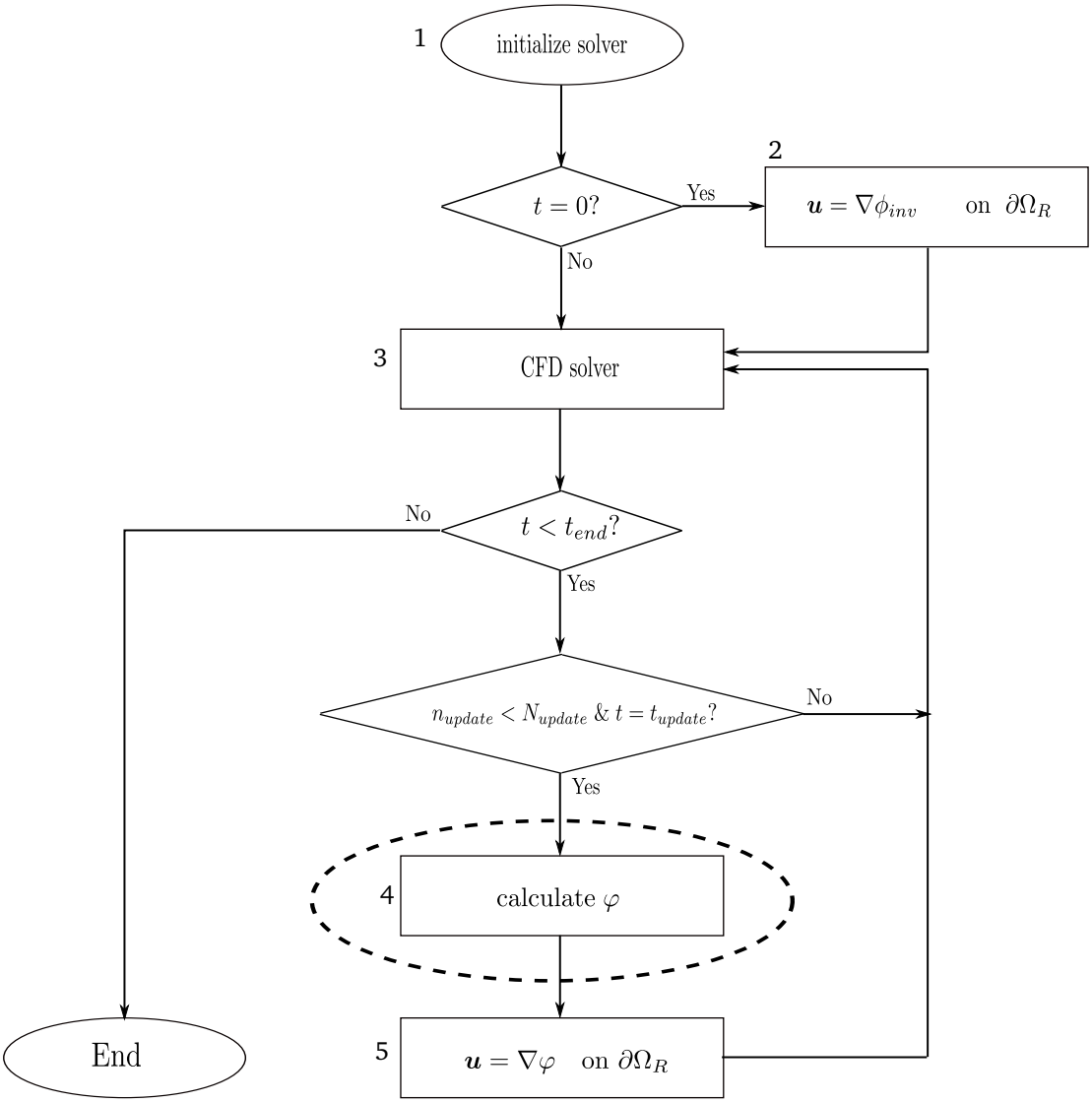

Figure 3.2: Unsteady velocity decomposition algorithm

3.3.2 Instantaneous Velocity Based Approach

When the unsteadiness is present in the whole flow field, the total velocity field after velocity decomposition is shown in Eq.(3.17).

$$\boldsymbol{u}(\boldsymbol{x},t) = \nabla\varphi(\boldsymbol{x},t) + \boldsymbol{w}(\boldsymbol{x},t) \tag{3.17}$$

Both $\boldsymbol{w}$ and φ are time dependent. So the instantaneous velocity field can be used to calculate the viscous potential. This is to calculate the viscous potential using the instantaneous velocity generated in Navier-Stokes sub-problem. It is functionally similar to the approach used in *Edmund* (2012) and *Rosemurgy* (2014). The calculation executed in this method is the complete process within step 4. Steps of the instantaneous velocity Based method are described below:

4.1 Calculate the vorticity thickness, δ, based on the magnitude of the vorticity, $\boldsymbol{\omega} = \nabla \times \boldsymbol{u}$. The details of this procedure are discussed in 3.3.2.1.

4.2 Iterate the following steps until the convergence criteria for the vortical velocity is met.

(a) Calculate the vortical velocity, $\boldsymbol{w}^{(i)} = \boldsymbol{u} - \nabla\varphi^{(i)}$. (The superscripts, (i), denote the iteration counter.)

(b) Calculate the strength of the source distributions using the viscous boundary condition, Eq.(3.23).

(c) Check if the convergence criteria is met, go to step 5 of velocity decomposition algorithm in previous section. If not, go back to step 4.2(a).

In this method, The update time, t_{update}, can be specified by the user. The user can specify the update time, t_{update}, by setting the interval between updates, as stated in

Eq.(3.18).

$$t_{\text{update}} = t_0 + n_{\text{update}} \cdot dt_{\text{update}} \tag{3.18}$$

where t_0 is the time the user want to start the update, n_{update} is the update counter shows the number of updates have been made, dt_{update} is the time interval between updates which means how frequently updates should be made. For this method, the user can also turn off the update time setting and have the solver update in every time step of the simulation. By doing this, the simulation accuracy is increased by paying the price of a higher computational cost. The viscous boundary condition discussed in chapter II is restated in Eq.(3.19) for convenience. Different than the boundary condition in chapter III, the term with $w_n(\delta)$ still needs to be included, because it is non-zero before the correct viscous potential is achieved.

$$\begin{aligned} \frac{\partial \varphi^{(i+1)}}{\partial n} &= -\int_0^{\delta} \left(\frac{\partial w_t^{(i)}}{\partial t} \right) \mathrm{d}n \qquad \text{on } \partial\Omega_B \\ &= -w_n^{(i)}(0) + w_n^{(i)}(\delta) \end{aligned} \tag{3.19}$$

The first term on the right hand side of Eq.(3.19) can be expressed as Eq.(3.22), which is derived from Eq.(3.20)-(3.21). The velocity vector equals to zero in Eq.(3.21), because of the non-slip condition.

$$\boldsymbol{w} = \boldsymbol{u} - \nabla\varphi \tag{3.20}$$

$$= \cancelto{0}{\boldsymbol{u}} - \nabla\varphi \qquad \text{on } \partial\Omega_B \tag{3.21}$$

$$w_n(0) = -\frac{\partial \varphi}{\partial n} \tag{3.22}$$

With the expression in Eq.(3.22), the viscous boundary condition, Eq.(3.19), can be stated as in Eq.(3.23). The normal component of the vortical velocity at δ can be

treated as a correction of the boundary condition from the previous iteration.

$$\frac{\partial \varphi^{(i+1)}}{\partial n} = \frac{\partial \varphi^{(i)}}{\partial n} + w_n^{(i)}(\delta) \tag{3.23}$$

The detailed discussion of this formulation of the viscous boundary condition can be found in *Rosemurgy* (2014).

The convergence criteria used by the iteration is shown in Eq.(3.24).

$$\epsilon_{\varphi}^{(i)} = \frac{\left| \|w_n^{(i)}(\delta)\|_\infty - \|w_n^{(i-1)}(\delta)\|_\infty \right|}{\|w_n^{(i)}(\delta)\|_\infty} < \tilde{\epsilon}_{\varphi} \tag{3.24}$$

The infinity norm is used to judge the convergence of the iteration. $\tilde{\epsilon}_{\varphi}$ is the tolerance set by the user.

3.3.2.1 Determination of Vorticity Thickness

At step 4.1 of section 3.3.2, a procedure is applied to determine the vorticity thickness, which is a scalar distance, δ, away from each panel center in the panel normal direction. This procedure is essentially the same as the one that is used by *Rosemurgy* (2014). The steps of the procedure are described below:

4.1.1 Sample from the panel center to a distance, δ_{max}, and find the maximum of the vorticity magnitude, $|\boldsymbol{\omega}|_{max}$ for each panel.

4.1.2 If $|\boldsymbol{\omega}|_{max}$ is smaller than a threshold value, $|\boldsymbol{\omega}|_{\alpha}$, that set by the user to eliminate fictitious numerical fluctuations, the maximum vorticity magnitude is set to zero.

4.1.3 Sample from the location, where the maximum vorticity magnitude was found, to δ_{max}. Find the location where vorticity magnitude is smaller than a threshold value, $|\boldsymbol{\omega}|_{\text{limit}}$.

4.1.4 If the minimum of vorticity magnitude along the sample line is larger than $|\boldsymbol{\omega}|_{\text{limit}}$, δ is set to zero and the inviscid non-penetration boundary condition is applied for this panel.

For unsteady flow, Step 4.1.2 is added in addition to the original procedure to prevent fictitious numerical fluctuations at the area where the vorticity has not yet developed. The threshold value, $|\boldsymbol{\omega}|_\alpha$, can be set as a fraction of the magnitude of the free-stream velocity divided by the body length, as in Eq.(3.25).

$$|\boldsymbol{\omega}|_\alpha = \alpha_\omega \frac{|U_\infty|}{L_B} \tag{3.25}$$

where α_ω is the fraction value can be set by the user, L_B is the body length.

The threshold value, $|\boldsymbol{\omega}|_{\text{limit}}$, in step 4.1.3 can be set as in Eq.(3.26).

$$|\boldsymbol{\omega}|_{\text{limit}} = \beta_\omega |\boldsymbol{\omega}|_{max} \tag{3.26}$$

where β_ω is a factor set by the user.

3.3.3 Time-averaged Velocity Based Approach

When the unsteadiness is mainly confined in a small region around the body, this means that the flow outside the vortical region is weakly time dependent, or even steady. Then velocity decomposition of the total velocity field can be transform to Eq.(3.27).

$$\begin{aligned} \boldsymbol{u}(\boldsymbol{x}, t) &= \nabla\varphi(\boldsymbol{x}, t) + \boldsymbol{w}(\boldsymbol{x}, t) \\ &\approx \nabla\varphi(\boldsymbol{x}) + \boldsymbol{w}(\boldsymbol{x}, t) \end{aligned} \tag{3.27}$$

Eq.(3.27) shows that the viscous potential velocity can be treated as a time invariant solution. Then the time-averaged velocity field can be used to calculate the viscous

potential for a considerable save in computational cost. The procedure of this method is similar with the instantaneous velocity based method except the following changes.

When using this method, the time of updates, t_{update}, is defined as in Eq.(3.28).

$$t_{\text{update}} = t_0 + (n_{\text{update}} + 1) \cdot T_{\text{avg}} \tag{3.28}$$

where t_0 is the start-time of the time averaging, T_{avg} is the averaging period of the time averaging, n_{update} is the update counter. The time-averaged velocity is calculated as in Eq.(3.29)

$$\overline{\boldsymbol{u}} = \frac{\sum_{i=1}^{N_{\text{time}}} (\boldsymbol{u}_i \cdot dt_i)}{T_{\text{avg}}} \tag{3.29}$$

$$T_{\text{avg}} = \sum_{i=1}^{N_{\text{time}}} dt_i \tag{3.30}$$

where N_{time} is the number of time steps, dt is the time step size. After the time-averaged velocity is calculated, it is used to replace the role of, $\boldsymbol{u}$, in the instantaneous velocity based method. The procedure to determine the vorticity thickness, δ, is the same as the one described in section 3.3.2.1, except the vorticity field is replaced by the mean vorticity field Eq.(3.31).

$$\overline{\boldsymbol{\omega}} = \nabla \times \overline{\boldsymbol{u}} \tag{3.31}$$

After the vorticity thickness is determined, the time-averaged velocity is used to calculate the vortical velocity Eq.(3.32).

$$\overline{\boldsymbol{w}} = \overline{\boldsymbol{u}} - \nabla\varphi \tag{3.32}$$

Then the mean vortical velocity, $\overline{\boldsymbol{w}}$ and the mean velocity field, $\overline{\boldsymbol{u}}$ is used throughout the iteration to calculate the viscous potential, instead of the instantaneous quantities.

The rest of the steps in the time-averaged velocity based method is similar to those in the instantaneous velocity based method.

3.3.4 Summary of Parameters in Unsteady Velocity Decomposition Solver

In this section, user-specified parameters in the unsteady velocity decomposition solver are summarized. For the velocity decomposition algorithm, there are 4 parameters in total, that govern the algorithm. They are listed in table 3.1, where the U_{inst} and U_{mean} represents respectively the instantaneous velocity and time-averaged velocity based method.

Parameters	Function
t_0	the time of the first update (U_{inst}) the start-time of averaging (U_{mean})
N_{update}	the total number of updates
dt_{update}	the time interval between update (U_{inst})
T_{avg}	the period of the time averaging (U_{mean})

Table 3.1: The parameters for the velocity decomposition updates

In the calculation of the viscous potential, four parameters can be controlled by the user. They are listed in table 3.2.

Parameters	Function
$\tilde{\epsilon}_{\varphi}$	the convergence criteria of vortical velocity
δ_{max}	the maximum sample distance for searching $\|\omega\|_{max}$
α_{ω}	the factor control the vorticity filter value, $\|\omega\|_{\alpha}$
β_{ω}	the factor for calculate the negligible vorticity magnitude

Table 3.2: The parameters for viscous potential calculation

To account for the viscous effects in the wake, the wake surface also need to be discretized. This is done using the same procedure described in *Rosemurgy* (2014). The wake surface is discretized by wake panels, starting from the trailing edge of the body to some distance, L_{wake}, downstream. N_{wake} is the total number of wake panel. ζ_{wake} is the growth rate of the wake panel length. Δ_{wake} is the length of the first wake

panel. The length of each panel is calculated as a geometric series, Eq.(3.33).

$$l_{\text{wake,i}} = \Delta_{\text{wake}}(1 + \zeta_{\text{wake}})^i \tag{3.33}$$

CHAPTER IV

Unsteady Velocity Decomposition Results

In this Chapter, two cases: two-dimensional laminar flow over a finite-length flat plate and a circular cylinder, are simulated to demonstrate the method of unsteady velocity decomposition discussed in preceding chapters. The unsteady viscous potential is studied first to justify it can be used as boundary condition on the reduced domain. Unsteady viscous potential velocity is calculated based on the largest domain and compared with the Navier-Stokes solution from fully viscous CFD simulation in the largest domain. Then, the effect of the outlet boundary location is investigated to determine a appropriate reduced domain size. Lastly, results of simulation in a significantly reduced domain using unsteady velocity decomposition method are generated and discussed.

4.1 Laminar Flow Over Finite Flat Plate

In this section, unsteady velocity decomposition method is applied to the flow over a finite-length flat plate. The Reynolds number based on the flat plate length, L, is $Re = 2000$. The flat plate is located at the center of the bottom boundary of the domain. The bottom boundary is specified as three parts. The parts located behind and in front of the flat plate is the center plane boundary, $\partial\Omega_{\mathrm{CP}}$, at which the slip boundary condition is applied. At the flat plate, $\partial\Omega_B$, the no-slip boundary

condition is applied. The free-stream flow is in the $x+$ direction, flowing from the inlet boundary $\partial\Omega_I$. The boundaries $\partial\Omega_I, \partial\Omega_F, \partial\Omega_O$ ares located at the distance, x_{extent}, away from the flat plate. The schematic sketch of the domain is shown in figure 4.1. And the boundary conditions for the Navier-Stokes problem are stated in equations (4.1).

$$
\begin{cases} \boldsymbol{u} = \boldsymbol{U_\infty} \\ \frac{\partial p}{\partial n} = 0 \end{cases} \quad on \quad \partial\Omega_I \quad and \quad \partial\Omega_F \tag{4.1}
$$

$$
\begin{cases} \frac{\partial \boldsymbol{u}}{\partial n} = 0 \\ p = 0 \end{cases} \quad on \quad \partial\Omega_O
$$

$$
\begin{cases} \boldsymbol{u} = 0 \\ \frac{\partial p}{\partial n} = 0 \end{cases} \quad on \quad \partial\Omega_B
$$

$$
\begin{cases} \frac{\partial u}{\partial n} = 0, \quad v = 0 \\ \frac{\partial p}{\partial n} = 0 \end{cases} \quad on \quad \partial\Omega_{\text{CP}}
$$

where n is the outward pointing normal direction, u, v is the horizontal and vertical component of the velocity vector.

The details of the largest computational grid are listed in table 4.1. Other computational grids used in this case are topologically identical as the largest computational grid in the common regions.

number of cells	Δx_{min}	Δz_{min}
88953	0.01	0.01

Table 4.1: The parameters of the largest computational grid

Even though this is an extremely simple problem, it is still a good test case to study velocity decomposition method for unsteady flow, because of the growth of the boundary layer during the start-up process due to the no-slip boundary condition

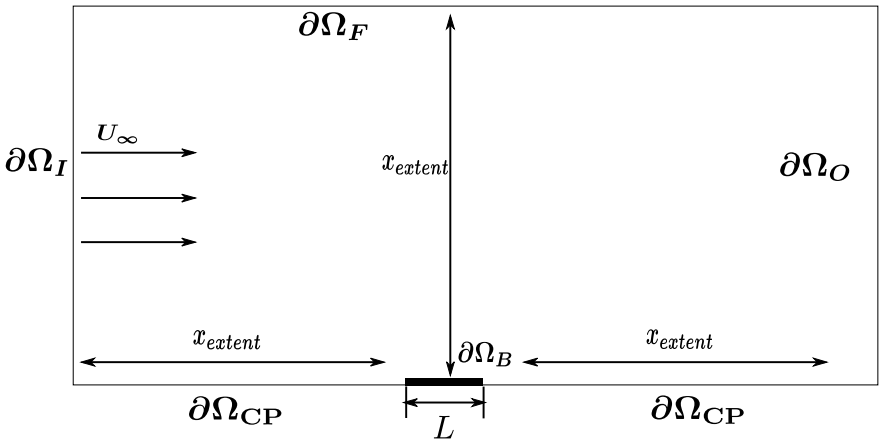

Figure 4.1: The domain of the flow over flat plate simulation

specified on flat plate. Its simplicity gives an unpolluted view of the velocity decomposition approach handling this instantaneous unsteadiness. It is worth knowing that, for conventional potential flow based method, the solution for this case equals to the free-stream velocity everywhere in the domain, while velocity decomposition provides the correct potential velocity that satisfies the Navier-Stokes equations outside the vortical region, as discussed in chapter II.

It is also a demonstration of the instantaneous velocity based approach to calculate the viscous potential discussed in chapter III. Because of the physics of the this problem, the boundary layer keeps growing before reaching steady state. During this process, vorticity is diffused away from the flat plate and transported downstream, after it is generated. This means a vortical region with changing shape and area. And it will affect the solution even outside the vortical region. So it is important to know if the unsteady velocity decomposition method can capture all the viscous effects.

4.1.1 Unsteady Viscous Potential

This section focuses on calculating a viscous potential velocity that matches with the benchmark solution (the Navier-Stokes solution in the largest domain). The

unsteady viscous potential velocity is calculated based on the Navier-Stokes solution of the largest domain ($x_{\text{extent}} = 1000L$, L is the flat plate length). The parameters for calculating the viscous potential are set using the discussion in *Edmund* (2012) and *Rosemurgy* (2014) as guidelines. The setting of parameters is listed in table 4.2. The number of wake panels is set to 0, $N_{\text{wake}} = 0$, while both the center plane and the flat plate are represented using body panel. This can be used to generate correct results because of the special nature of this problem and the viscous potential. For the viscous boundary condition of viscous potential discussed in chapter II, it is effectively to alter the shape of body based on viscous effects like boundary layer and wake. So for this case, the panels at the center plane boundary in front of the flat plate have no effect on the flow. The value of δ_{max} is set as a relatively large value to ensure that the boundary layer and wake is completed included during the calculation of viscous potential.

Parameters	Value
δ_{max}/L	5
N_{wake}	0
ϵ_{φ}	0.01
β_{ω}	0.01
α_{ω}	1e-3

Table 4.2: The parameter value for viscous potential calculation of flow over flat plate

Due to the unsteadiness of the flow, a non-dimensional time t^* is defined for convenience.

$$t^* = \frac{t}{t_{ref}} = \frac{tU_\infty}{L} \tag{4.2}$$

where $t_{ref} = \frac{L}{U_\infty}$, which is the time that it takes for the flow to travel one body length.

The profile of streamwise velocity at $z/L = 0.3$ is shown in figure 4.2(a). For conciseness, only the solutions of $x/L \in [-10 : 20]$ are shown. The viscous potential velocity $\varphi_{,x}$ agrees very well with the Navier-Stokes solution for $x/L < 6$. After that, two solutions show completely different trends. The reason causing this discrepancy

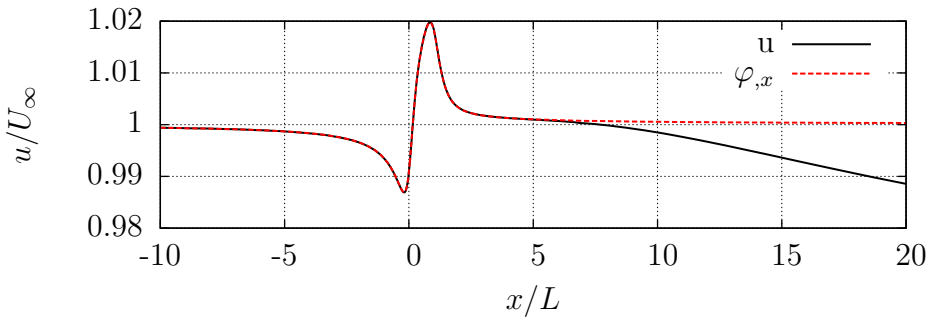

(a) Streamwise velocity profile at $z/L = 0.3$

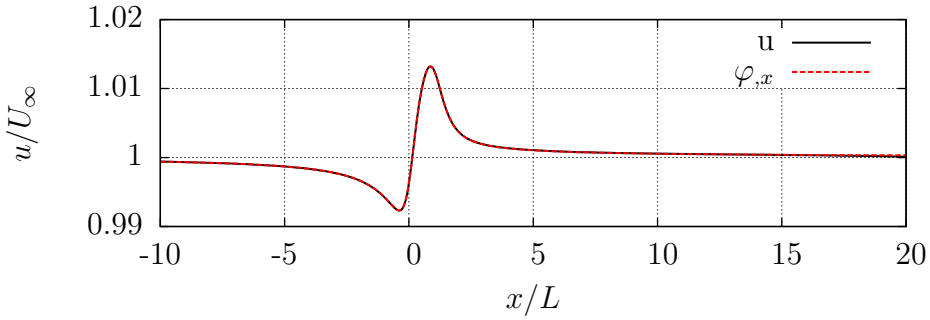

(b) Streamwise velocity profile at $z/L = 0.5$

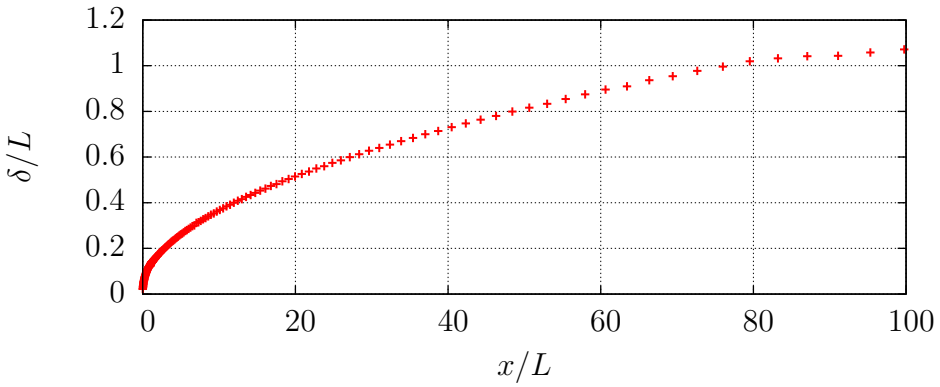

(c) Vorticity thickness

Figure 4.2: Profiles of streamwise velocity and vorticity thickness at $t^* = 100$, ($\varphi_{,x}$ is the streamwise component of viscous potential velocity, u is that of the Navier-stokes solution, U_∞ is the free-stream velocity)

is that the sample line $z/L = 0.3$ is inside the vortical region after around $x/L = 6$. As can be found in figure 4.2(c), the vorticity thickness δ/L at $x/L = 6$ is around 0.3. To verify this, a profile of streamwise velocity at $z/L = 0.5$, which is outside the vortical region at $x/L = 20$ is generated. The viscous potential velocity overlaps with

the Navier-Stokes solution, as shown in figure 4.2(b).

The streamwise velocity profiles at $x/L = 0, 0.5, 1, 5$ are shown in figure 4.3. The two solutions do not agree within a small distance to the flat plate due to the vorticity in boundary layer and wake, while in the rest of the area, the viscous potential velocity almost overlaps with the Navier-Stokes solution for all positions shown.

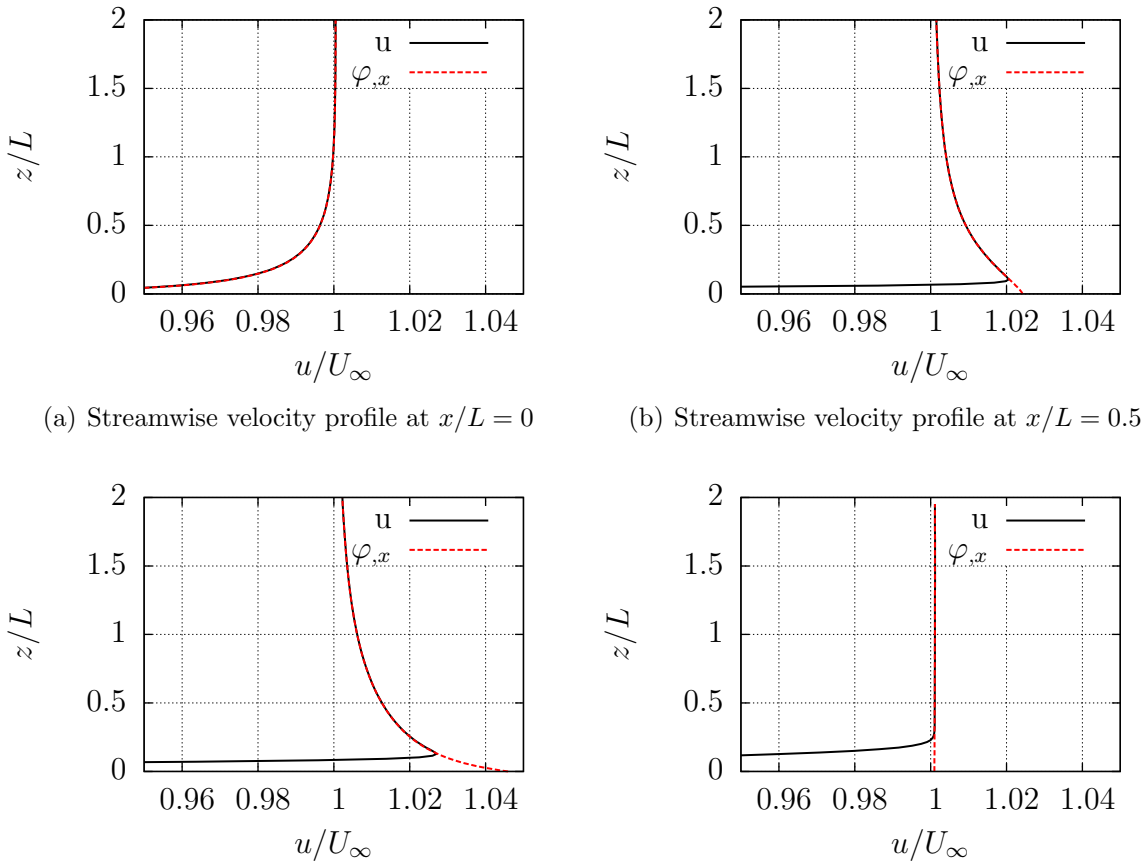

(a) Streamwise velocity profile at $x/L = 0$

(b) Streamwise velocity profile at $x/L = 0.5$

(c) Streamwise velocity profile at $x/L = 1$

(d) Streamwise velocity profile at $x/L = 5$

Figure 4.3: Vertical profiles of streamwise velocity at $t^* = 100$

To investigate if the unsteady velocity decomposition can generate a time accurate viscous potential solution that matches the Navier-Stokes solution, the time history of the solution needs to be studied. As shown in figure 4.4, the time history of the streamwise viscous potential velocity is compared with the Navier-Stokes solution at three different locations, $(0, 0.3L), (0.5L, 0.3L), (1L, 0.3L)$. The vertical coordinate is

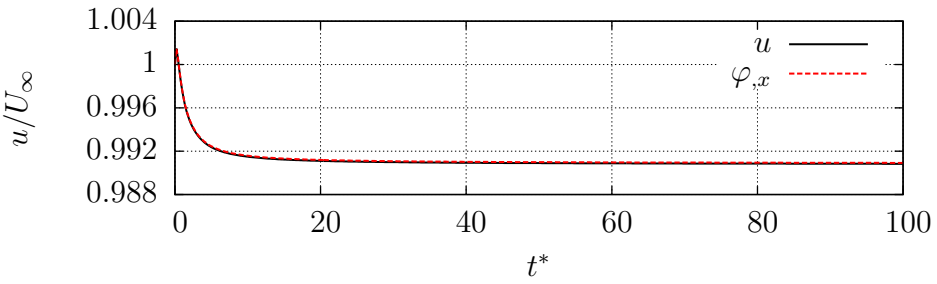

(a) Streamwise velocity time history at $(0, 0.3L)$

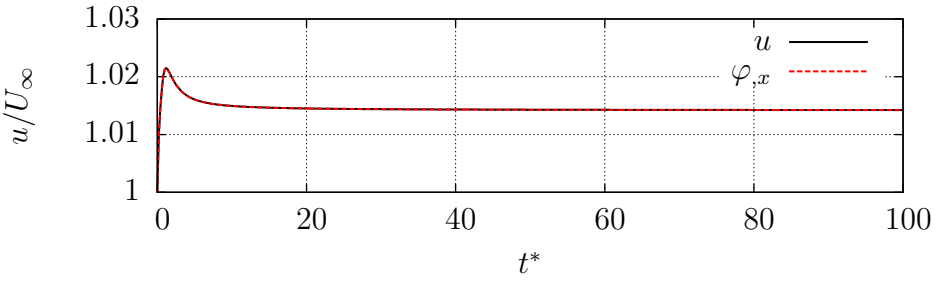

(b) Streamwise velocity time history at $(0.5L, 0.3L)$

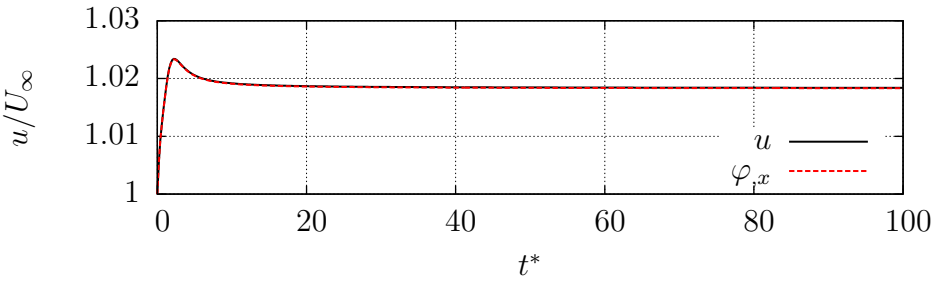

(c) Streamwise velocity time history at $(1L, 0.3L)$

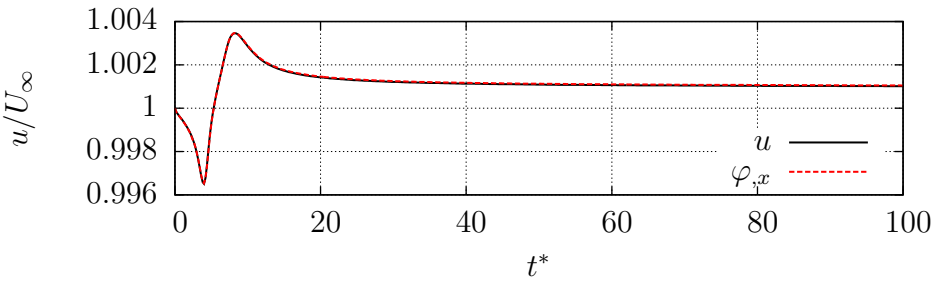

(d) Streamwise velocity time history at $(5L, 0.3L)$

Figure 4.4: The time histories of streamwise velocity

chosen to make sure the sample points are outside the vortical region, only in which the viscous potential is physical. As can be seen, the viscous potential velocity almost

overlaps with the Navier-Stokes solution at all time instants. As the viscous potential velocity agrees well with the Navier-Stokes solution, it is possible to use it as the boundary condition at the inlet and far-field boundaries of the reduced domain.

4.1.2 Effect of Outlet Boundary Location

Since the viscous wake is rotational, the velociy decomposition can only be applied to the inlet and farfield boundary ($\partial\Omega_I, \partial\Omega_F$). To minimize the influence of the outlet boundary condition, the outlet boundary need to be set far away downstream.

One of the advantages of velocity decomposition approach is to reduce the computational domain for the Navier-Stokes problem. So it would be useful to investigate the effect of the outlet boundary location. To be consistent, the meshes used for this

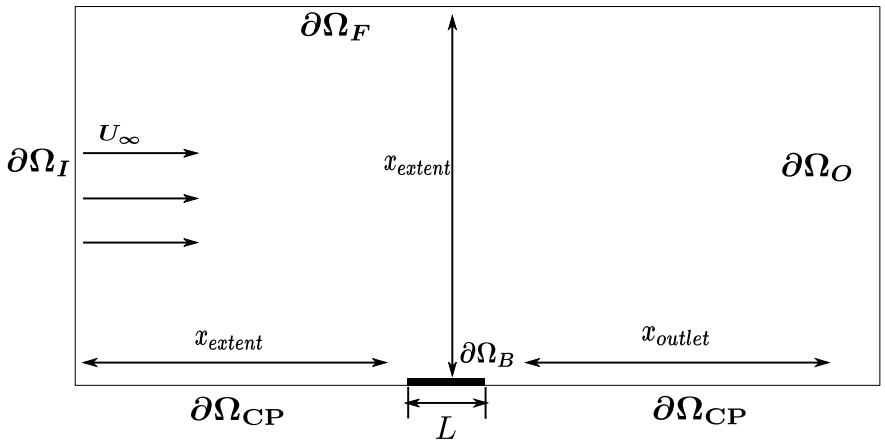

Figure 4.5: Flow domain of outlet boundary location study

study are topologically identical in the common regions as the large domain in last section. As shown in figure 4.5, the computational domain is very similar to the large domain. The only difference is the distance between the flat plate and the outlet boundary, x_{outlet}. The study of the outlet boundary location in this work ranges from $x_{\text{outlet}}/L = 500$ to $x_{\text{outlet}}/L = 1$. All other settings are the same as the Navier-Stokes problem described in last section.

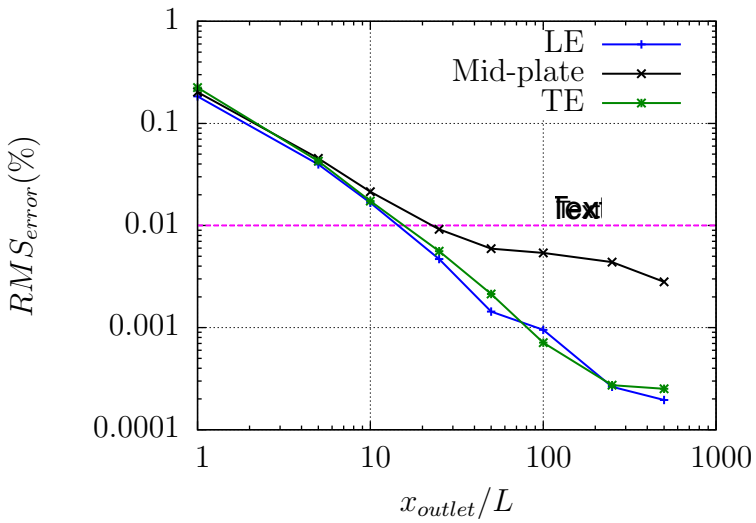

Figure 4.6: The effect of outlet boundary location(LE, Mid-plate, TE, represents the locations at $(0, 0.3L), (0.5L, 0.3L), (1L, 0.3L)$)

There are three metrics to evaluate the effect of the outlet boundary location. They are the root mean square errors of the streamwise velocity for $t^* \in [0 : 100]$ at three different locations. The three locations to sample the streamwise velocity are $(0, 0.3L), (0.5L, 0.3L), (1L, 0.3L)$. The solution in the largest domain $x_{\text{extent}}/L = 1000$ is used as baseline solution. The root mean square errors are calculated as in stated in equation (4.3).

$$RMS_{error} = \frac{1}{N_{\text{time}}} \sqrt{\sum_{i=1}^{N_{time}} \left(\frac{f_{x,i} - f_{1000L,i}}{f_{1000L,i}} \right)^2} \times 100\% \tag{4.3}$$

where f represents the variable that desired to calculated root mean square error with. In this case, f can be the streamwise velocity in those three locations. $f_{1000,i}$ is the value from the largest domain. N_{time} is the total number of time steps. 0.01% is used as a error bound for all the values. As shown in figure 4.6, it can be found that for the case $x_{\text{outlet}}/L = 25$, the root mean square error of all the values is below the 0.01%. Hence, $x_{\text{outlet}}/L = 25$ is the smallest distance to outlet boundary without affecting the accuracy of the solution. So $x_{\text{outlet}}/L = 25$ is selected as the outlet

boundary location for the reduced domain in the next section.

4.1.3 Unsteady Velocity Decomposition On Reduced Domain

From the results of preceding sections, it is confident that unsteady velocity decomposition method is capable of providing correct results while considerably reducing the domain size. The computational domain for this case is significantly reduced from $x_{\text{extent}}/L = 1000L$ to $x_{\text{extent}}/L = 0.8$, while x_{outlet}/L is set as 25 based on the study from last section.

The settings of the parameters for unsteady velocity decomposition is show in table 4.3. The parameters not shown in the table is set as the same as in table 4.2. It is worth knowing that δ_{max} is reduced to 0.6. As from figure 4.2(c), at $x/L = 25$, the vorticity thickness is $\delta/L \approx 0.6$.

Parameters	Value
N_{update}	200
$T_{\text{update}}/t_{ref}$	0.2
δ_{max}	0.6

Table 4.3: The parameter value for viscous potential calculation of flow over flat plate

For the results presented in figure 4.7-4.9, the Navier-Stokes solutions on the largest domain and reduced domain are denoted as "NSL" and "NSR"respectively. The Navier-Stokes solutions on the reduced domain are also compared to show the improvement by applying velocity decomposition. The velocity decomposition results, that use the same parameter but updated in every time step, are also calculated and denoted as "VD2", while the velocity decomposition results updated based on the parameter in table 4.3 denoted as "VD1".

As shown in figure 4.7-4.8, all the streamwise velocity profile of the velocity decomposition solutions at $t^* = 100$ agrees well with the Navier-Stokes solution, while the Navier-Stokes solutions in the reduced domain are over-predicted. Figure 4.9 shows the time histories of streamwise velocity at four location, $(0, 0.3L)$, $(0.5L, 0.3)$,

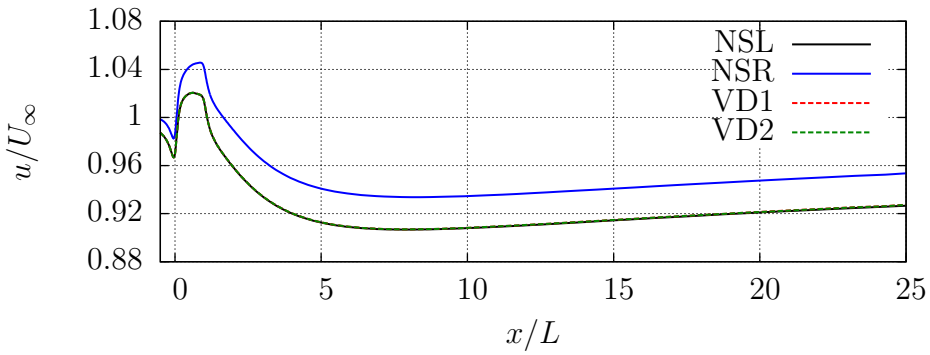

(a) Streamwise velocity profile at $z/L = 0.1$

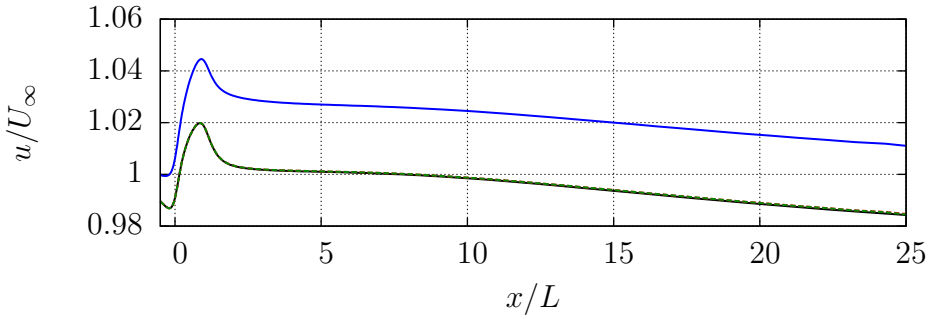

(b) Streamwise velocity profile at $z/L = 0.3$

Figure 4.7: Horizontal profiles of streamwise velocity at $t^* = 100$

$(1L, 0.3L)$, $(5L, 0.3L)$. Since the flow becomes steady for $t^* > 20$, only the time history for $0 \leq t^* \leq 20$ is shown. For the VD1 solution before $t^* = 5$, there is some overshoot of the solutions. After that, the solutions are quickly corrected by the viscous potential velocity boundary condition. On the other hand, the VD2 solutions shows remarkable agreement with the Navier-Stokes solutions in the large domain. Even though the computational cost of VD2 solutions is higher than that of VD1, it is still much more efficient than that of the Navier-Stokes large domain solutions.

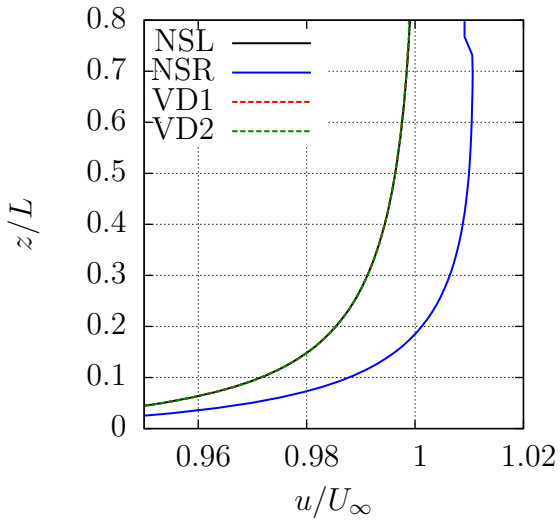

(a) Streamwise velocity profile at $x/L = 0$

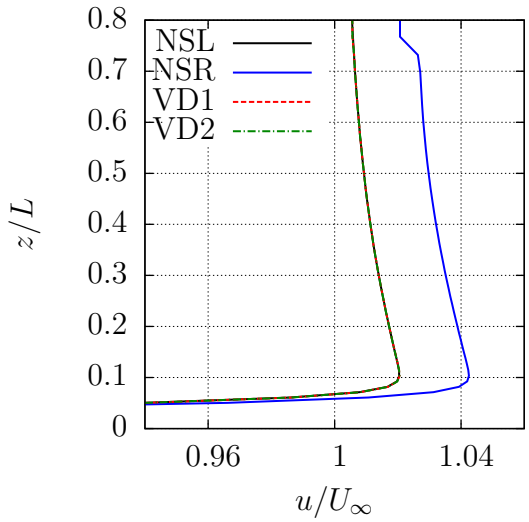

(b) Streamwise velocity profile at $x/L = 0.5$

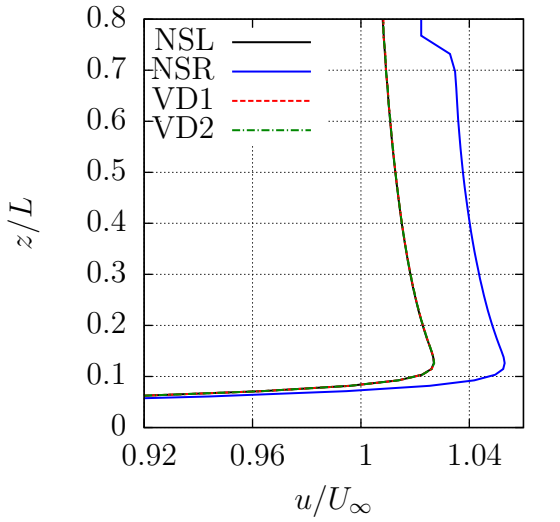

(c) Streamwise velocity profile at $x/L = 1$

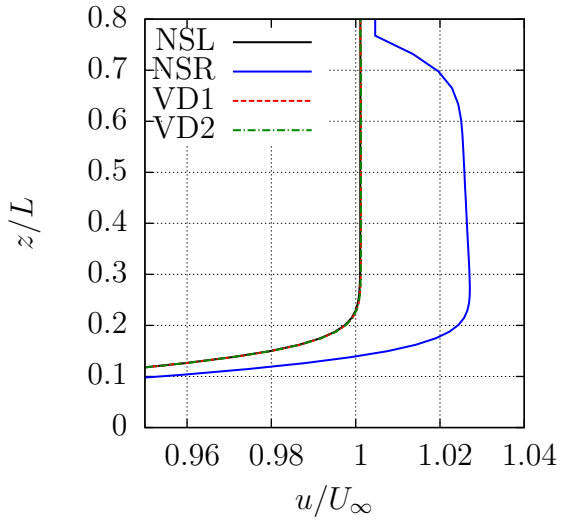

(d) Streamwise velocity profile at $x/L = 5$

Figure 4.8: Vertical profiles of streamwise velocity at $t^* = 100$

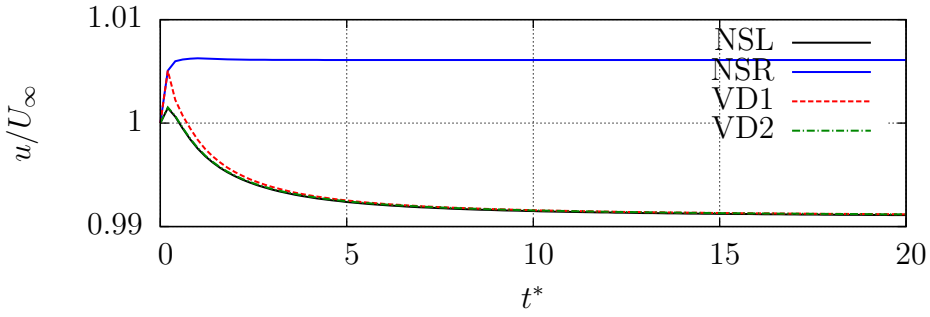

(a) Streamwise velocity time history at $(0, 0.3L)$

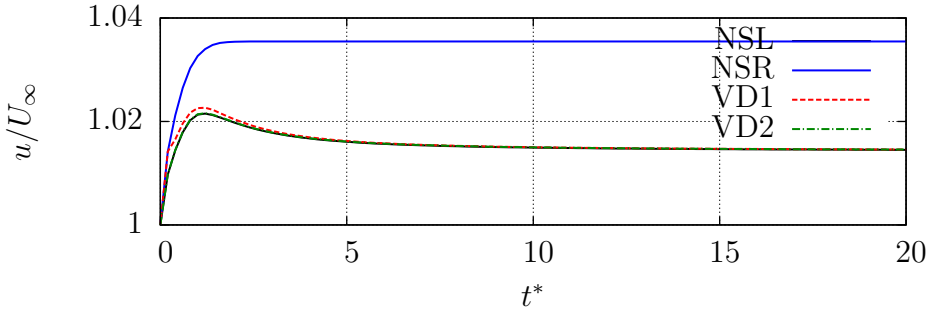

(b) Streamwise velocity time history at $(0.5L, 0.3L)$

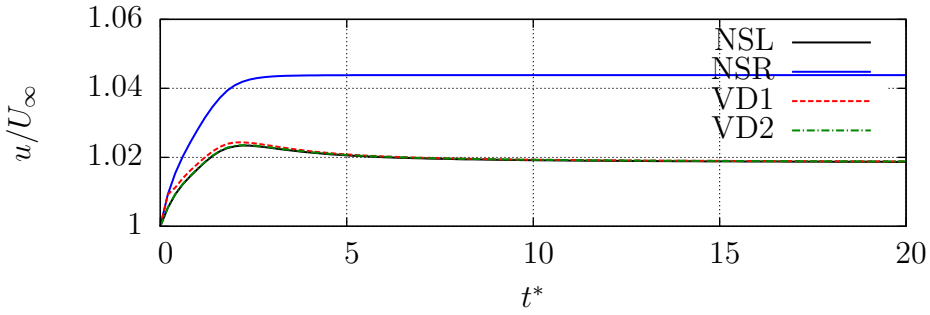

(c) Streamwise velocity time history at $(1L, 0.3L)$

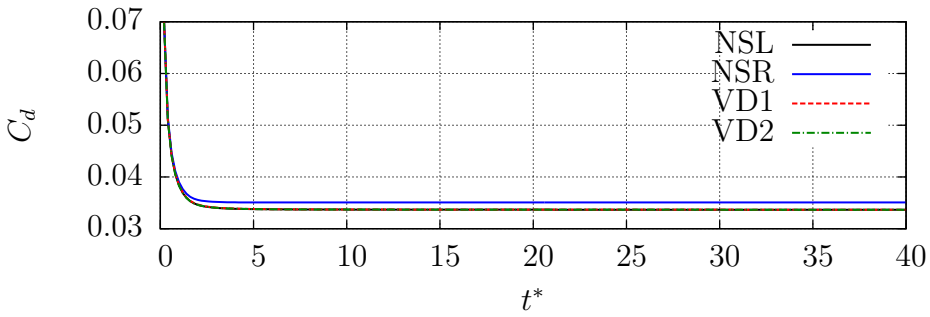

(d) Drag coefficient time history

Figure 4.9: The time histories of streamwise velocity and drag coefficient

4.2 Laminar Flow Over Cylinder

In this section, unsteady velocity decomposition method is applied to the flow over a circular cylinder. The Reynolds number based on the cylinder diameter, D, is $Re = 140$. The cylinder is located at the center of the domain. At the cylinder surface, $\partial\Omega_B$, the no-slip boundary condition is applied. The free-stream flow is in the $x+$ direction, flowing in from the inlet boundary $\partial\Omega_I$. The boundary $\partial\Omega_I, \partial\Omega_F, \partial\Omega_O$ is located x_{extent} away from the cylinder. The schematic sketch of the domain is shown in figure 4.10. And the boundary conditions for the Navier-Stokes problem are stated in equations (4.4).

$$\begin{cases} \boldsymbol{u} = \boldsymbol{U_\infty} \\ \frac{\partial p}{\partial n} = 0 \end{cases} \quad on \quad \partial\Omega_I \quad and \quad \partial\Omega_F \tag{4.4}$$

$$\begin{cases} \frac{\partial \boldsymbol{u}}{\partial n} = 0 \\ p = 0 \end{cases} \quad on \quad \partial\Omega_O \tag{4.5}$$

$$\begin{cases} \boldsymbol{u} = 0 \\ \frac{\partial p}{\partial n} = 0 \end{cases} \quad on \quad \partial\Omega_B \tag{4.6}$$

The details of the largest computational grid are listed in table 4.4. Other computational grids used in this case are topologically identical as the largest computational grid in the common regions.

number of cells	$\Delta x_{\min}$	$\Delta z_{\min}$
176584	0.03	0.03

Table 4.4: The parameters of the largest computational grid

The physics of laminar flow over a circular cylinder has been extensively studied in the literature. The Reynolds number chosen for this case is within the range to generate the Von Kármán vortex street. This case would be a ideal test case to

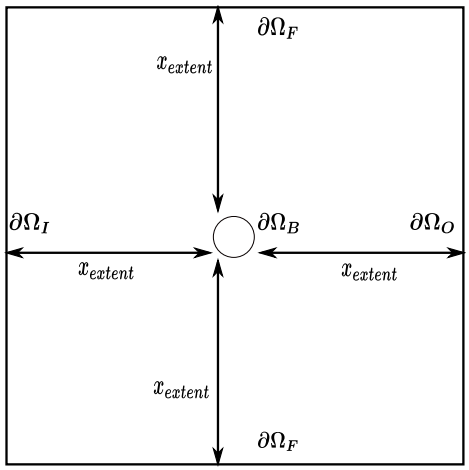

Figure 4.10: The domain of the flow over cylinder simulation

study the capability for unsteady velocity decomposition approach to handle unsteady separation flow around a blunt body. It is well known that the paradox of the inviscid potential solution in flow over cylinder, which is essentially unphysical. So the inviscid potential method is generally not applicable for massively separation flows. This makes it a interesting challenge for the unsteady velocity decomposition method.

In *Edmund* (2012), promising results are shown for the steady laminar flow over cylinder in a very low Reynolds number, $Re = 60$. It is a good demonstration of the capability of velocity decomposition method handling flow with massive amount of separation. However, for $Re = 60$, there is no Von Kármán vortex street and the flow is steady.

In the case studied in this work, after the flow has developed, the oscillating flow around the cylinder shows a steady frequency. A strong periodicity presents in the flow field. This would be a appropriate condition to use the time-averaged velocity based method (discussed in chapter III) to calculate the viscous potential. Hence, this section would investigate the feasibility of this U_{mean} based approach.

4.2.1 Unsteady Viscous Potential

In order to apply the viscous potential velocity, convincing agreement outside the vortical region needs to be found between the viscous potential velocity and the solution from the Navier-Stokes solution in a large domain, ($x_{extent} = 1000D$ is selected). Since the U_{mean} based approach described in III is applied to generate the viscous potential, the viscous potential velocity is compared with the time averaged velocity, $\overline{\boldsymbol{u}}$, from large domain. $\overline{\boldsymbol{u}}$ is calculated as in equation (4.7) .

$$\overline{\boldsymbol{u}} = \frac{\sum_{i=1}^{N_{\text{time}}} (\boldsymbol{u}_i \cdot dt_i)}{T_N} \tag{4.7}$$

where N_{time} is the number of time steps of the simulation, T_N is the end time of the averaging. The parameters for calculating the viscous potential are set using the discussion in *Edmund* (2012) and *Rosemurgy* (2014) as guidelines. The setting of parameters is listed in table 4.5.

Parameters	Value
δ_{max}/D	10
N_{wake}	463
L_{wake}/D	200
ϵ_φ	0.01
β_ω	0.01
α_ω	1e-3

Table 4.5: The parameter value for viscous potential calculation of flow over cylinder

It is worth mentioning that calculating viscous potential based on $\overline{\boldsymbol{u}}$, instead of the instantaneous $\boldsymbol{u}$, has the advantage of reducing the computational cost as well as the difficulty for implementation. As shown in figure 4.11(a), the vorticity field is a typical Von Kármán vortex street, which can be troublesome because of the asymmetrical unsteady wake, while figure 4.11(b) shows the vorticity field generated by $\overline{\boldsymbol{u}}$, the wake is essentially steady and symmetrical. It still possesses the similar vorticity magnitude and vorticity thickness that velocity decomposition desired.

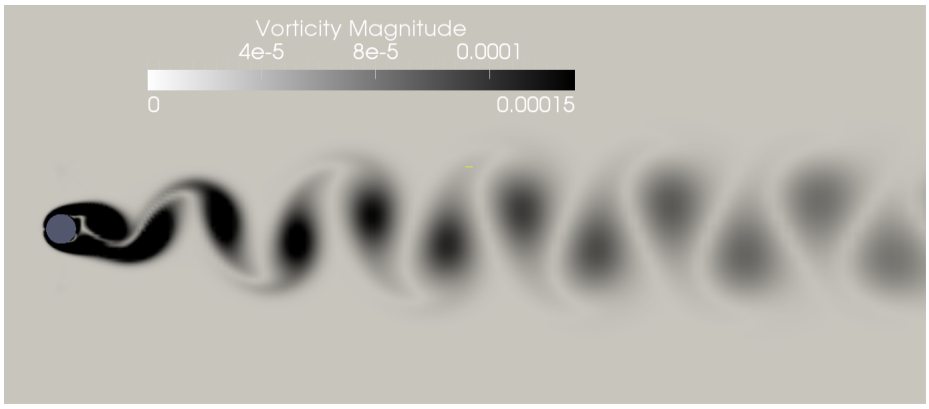

(a) Magnitude of vorticity

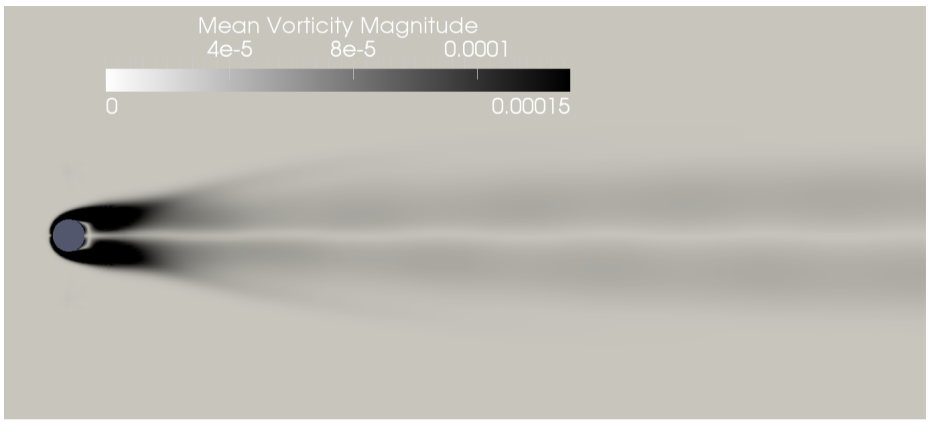

(b) Magnitude of mean vorticity

Figure 4.11: The contour of magnitude of vorticity and mean vorticity

To be able to generate a correct viscous potential based on $\overline{\boldsymbol{u}}$, two conditions need to be met. The first one is that the viscous potential velocity agrees with the $\overline{\boldsymbol{u}}$ field outside the vortical region. The other one is that the $\overline{\boldsymbol{u}}$ field is averaged in a way that can correctly represent the characteristics of the flow field.

In figure 4.12, velocity profiles of the streamwise component from viscous potential velocity and the instantaneous and time averaged Navier-Stokes solution in large domain are compared. Horizontal profile of the solutions at $z/D = \pm 6$ and vertical profile at $x/D = 0$ and 5 are shown, in figure 4.12. Figure 4.13 shows the time histories of those three solutions. As can be seen, $\varphi_{,x}$ agrees well with $\overline{u}$ outside the vortical region. Then the first condition is met, while the second condition is greatly relied on the averaging period for calculating the mean velocity field. This will be

discussed in section 4.2.3.

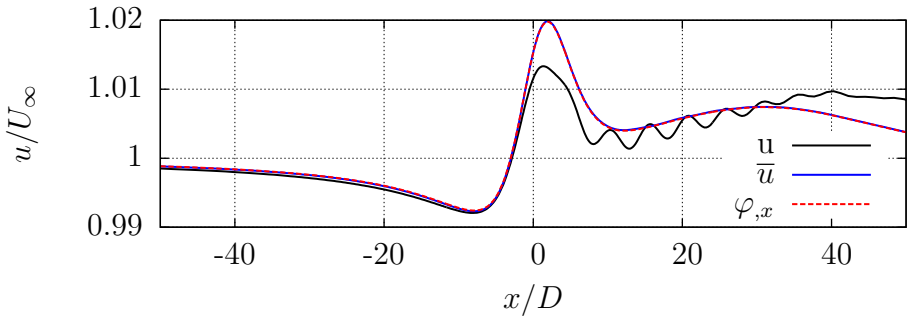

(a) Streamwise velocity profile at $z/D = 6$

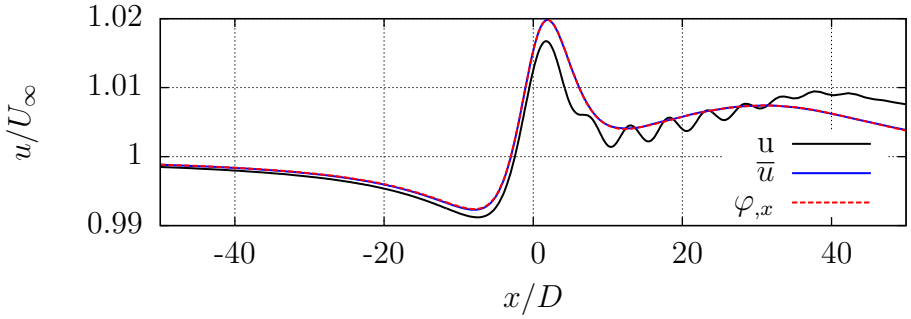

(b) Streamwise velocity profile at $z/D = -6$

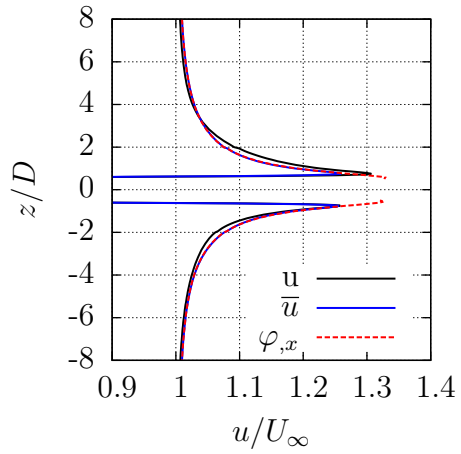

(c) Streamwise velocity profile at $x/D = 0$

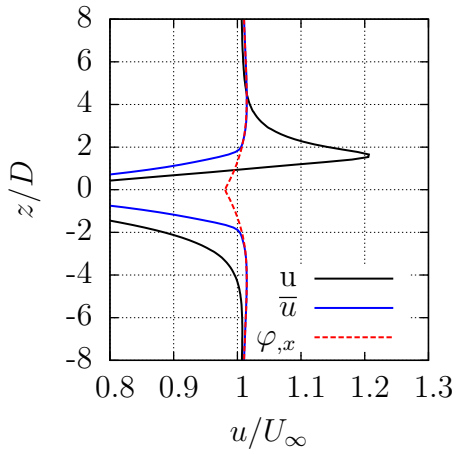

(d) Streamwise velocity profile at $x/D = 5$

Figure 4.12: Profiles of streamwise velocity at $t^* = 100$, ($\varphi_{,x}$ is streamwise component of viscous velocity, u and $\overline{u}$ is respectively the instantaneous and time averaged Navier-stokes solution)

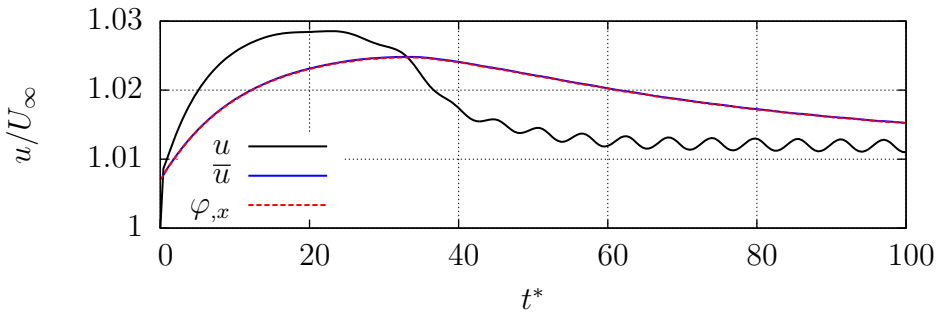

(a) Streamwise velocity time history at $(0, 6D)$

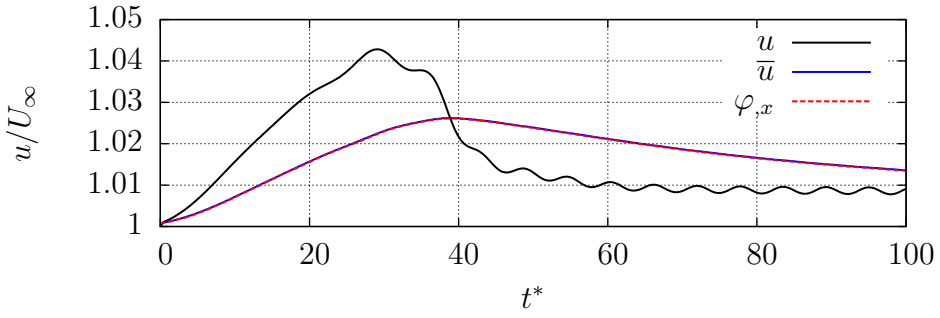

(b) Streamwise velocity time history at $(5D, 6D)$

Figure 4.13: The time histories of streamwise velocity

4.2.2 Effect of Outlet Boundary Location

Similar to the flat plate case, the effect of outlet boundary location need to be studied to determine the reduced domain size. To be consistent, the meshes used for this study are topologically identical in the common region as the large domain in last section.

As shown in figure 4.14, the computational domain is very similar to the large domain. The only difference is the distance between the center of the cylinder and the outlet boundary, x_{outlet}. The study of the outlet boundary location in this work ranges from $x_{\text{outlet}}/D = 250$ to $x_{\text{outlet}}/D = 25$. All other settings are the same as the Navier-Stoke problem described in section 4.2. There are three metrics to evaluate the effect of the outlet boundary location. They are the root mean square errors of the streamwise velocity at $t^* \in [0 : 100]$ at three different locations. The three locations

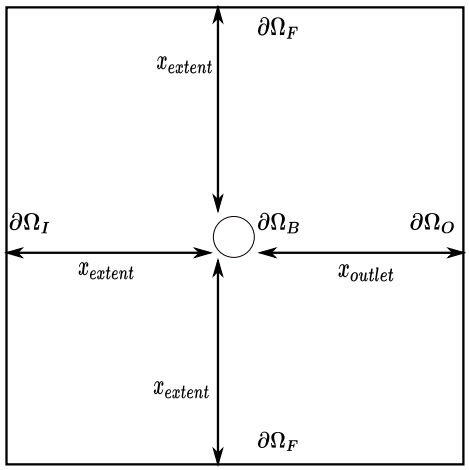

Figure 4.14: The domain for outlet boundary location study

to sample the streamwise velocity are $(0, 6D), (1D, 6D), (5D, 6D)$. The solutions in the largest domain $x_{\text{extent}}/D = 1000$ are used as baseline solutions. The root mean square errors are calculated as stated in equation (4.3).

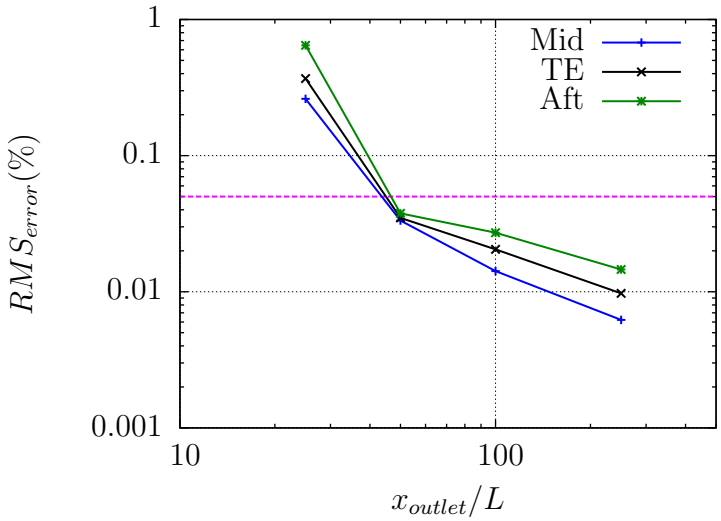

Figure 4.15: The effect of outlet boundary location(Mid, TE, Aft respectively represents the locations at $(0, 6D), (1D, 6D), (5D, 6D)$)

0.05% is used as a error bound for all the values. As shown in figure 4.15, it can be found that for the case $x_{\text{outlet}}/D = 50$, the root mean square error of all the values is below the 0.05%. Hence, $x_{\text{outlet}}/D = 50$ is the smallest distance to outlet boundary without affecting the accuracy of the solution. So $x_{\text{outlet}}/D = 50$ is selected as the

outlet boundary location for the reduced domain in the next section.

4.2.3 Unsteady Velocity Decomposition On Reduced Domain

The first condition for applying the time-averaged velocity based approach, which is the viscous potential velocity matches the mean velocity field outside the vortical region, is proved to be met in section 4.2.1. To satisfy the second condition, which is the mean velocity field can correctly represent the characteristics of the velocity field, $\overline{\boldsymbol{u}}$ needs to be averaged over integer times of the oscillation period after the flow shows a constant frequency. From the time histories in figure 4.13, the flow shows a relatively stable frequency for $t^* > 60$. The oscillating period is $T/t_{ref} \approx 5.5$. Then the averaging period is set correspondingly. With this setting, two conditions can be met. The velocity decomposition method is ready to be applied to this case.

Based on the vorticity thickness and influence of the outlet boundary location, the computational domain is reduced to $x_{\text{extent}} = 7D, x_{\text{outlet}} = 50D$. Since this case is used to demonstrate the ability of velocity decomposition solver to capture the Von Kármán vortex street, there is no intent to predict the start-up of the flow. Hence, only one update based on the instantaneous velocity is applied at $t^* = 60$. After that, 20 updates are made based on the time-averaged velocity field. The setting of the velocity decomposition parameters are shown in table 4.6.

Parameters	Value
N_{update}	200
T_{avg}/t_{ref}	5.5
t_{start}/t_{ref}	60
N_{wake}	325
L_{wake}/D	50
δ_{max}	6

Table 4.6: The parameter value for viscous potential calculation of flow over cylinder

Figure 4.16 shows the profile of streamwise velocity at $t^* = 200$ from velocity decomposition solver on a reduced domain and the Navier-Stokes solution on the

large domain, $x_{extent}/D = 1000$. To show the improvement of applying velocity decomposition method, the Navier-Stokes solutions on a reduced domain are shown as well. The oscillating amplitude and period match well with the Navier-Stokes solution in large domain, despite of the small difference in the phase of the solution. On the other hand, the Navier-Stokes solution in reduced domain is over-predicted.

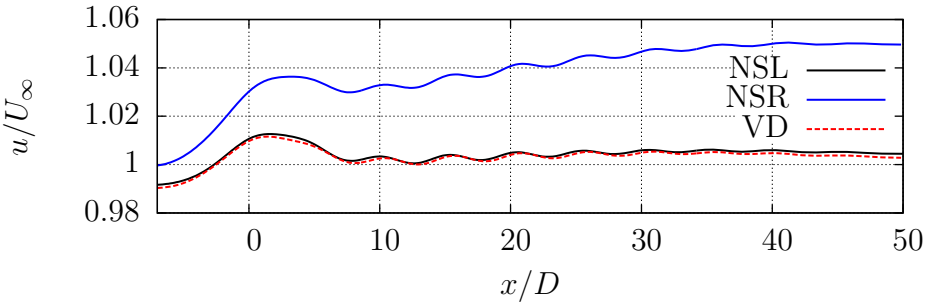

(a) streamwise velocity profile at $z/D = 6$

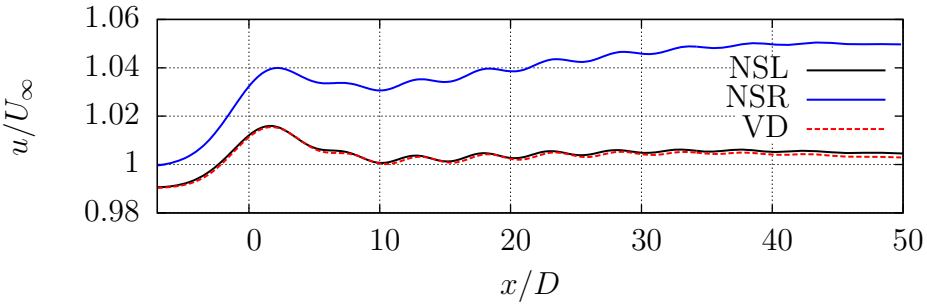

(b) streamwise velocity profile at $z/D = -6$

Figure 4.16: Horizontal profiles of streamwise velocity at $t^* = 200$

Due to the presence of phase difference, unlike preceding section, the velocity profiles on the vertical direction are not shown. However, this would not temper the analysis to velocity decomposition method, as good agreement is found when comparing the time histories of streamwise velocity in various locations and the drag coefficient in figure 4.17. It can be seen that all the time histories of velocity decomposition results in reduced domain match with the Navier-Stokes solutions after around $t^* \approx 100$. This means after around 7 updates in velocity decomposition, the solution is quickly corrected to match with the Navier-Stokes solution. So the time-averaged

velocity based method is able to provide accurate results.

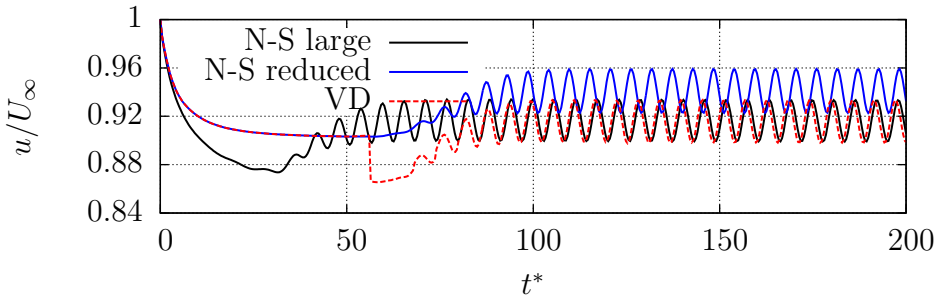

(a) Streamwise velocity time history at $(-1D, 1D)$

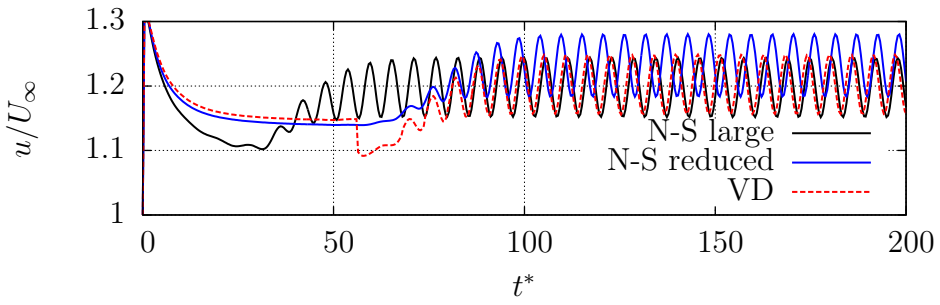

(b) Streamwise velocity time history at $(0, 1D)$

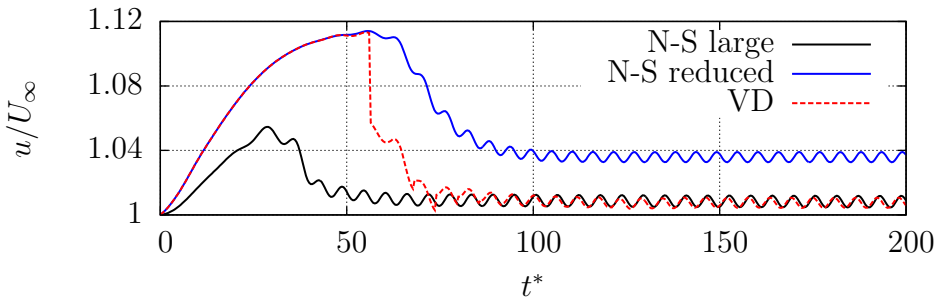

(c) Streamwise velocity time history at $(5D, 5D)$

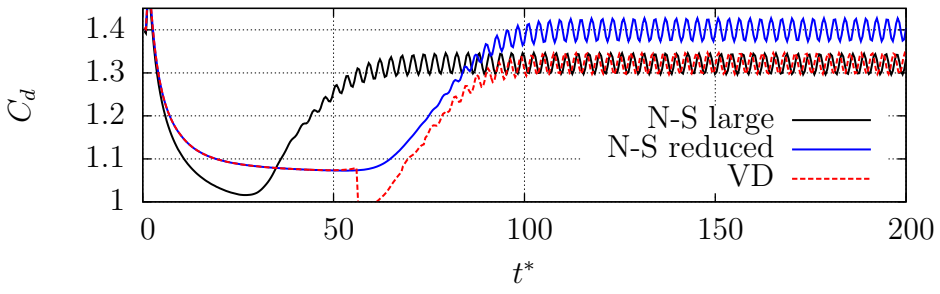

(d) Drag coefficient time history

Figure 4.17: The time histories of streamwise velocity and drag coefficient

CHAPTER V

Conclusion and Future Work

In this work, the velocity decomposition solver, developed by *Edmund* (2012) and *Rosemurgy* (2014), is extended to solve for unsteady flow problems. Two methods are proposed to solve for the viscous potential in the unsteady velocity decomposition algorithm. The instantaneous velocity based approach is applied when solving the two dimensional laminar flow over a finite flat plate. Good agreement between the velocity decomposition results and the results generated by a conventional CFD solver is shown. The time-averaged velocity based approach is applied to solve the two dimensional laminar flow over a circular cylinder with Von Kármán vortex street. Despite of differences in the phase of the solution, the amplitude and frequency of the oscillating wake predicted by the velocity decomposition solver matches well with those from conventional CFD solver. Even though only two-dimensional results are studied in this work, extension to three-dimensional cases is the next step, given the encouraging results presented by *Edmund* (2012). The velocity decomposition solver's ability to handle free-surface flow has been demonstrated by *Rosemurgy* (2014). Given the promising results for unsteady flow presented in this thesis, the velocity decomposition solver will be further developed to solve for three-dimensional turbulent flows with free-surface. The ultimate application of the velocity decomposition solver can be predicting the interaction among multiple bodies moving on the free-surface.

BIBLIOGRAPHY

BIBLIOGRAPHY

Campana, E., A. Di Mascio, P. Esposito, and F. Lalli (1995), Viscous-inviscid coupling in free surface ship flows, *International Journal for Numerical Methods in Fluids*, *21*(9), 699–722.

Chorin, A. J., and J. E. Marsden (1990), *A mathematical introduction to fluid mechanics*, vol. 3, Springer.

Eça, L., and M. Hoekstra (2009), On the numerical accuracy of the prediction of resistance coefficients in ship stern flow calculations, *Journal of marine science and technology*, *14*(1), 2–18.

Edmund, D. O. (2012), A velocity decomposition method for efficient numerical computation of steady external flows, Ph.D. thesis, The University of Michigan.

Edmund, D. O., K. J. Maki, and R. F. Beck (2011), An improved viscous/inviscid velocity decomposition method, in *26th International workshop on water waves and floating bodies, Athens*.

Edmund, D. O., K. J. Maki, and R. F. Beck (2013), A velocity-decomposition formulation for the incompressible navier–stokes equations, *Computational Mechanics*, *52*(3), 669–680.

Ferziger, J. H., and M. Perić (1996), *Computational methods for fluid dynamics*, vol. 3, Springer Berlin.

Hafez, M., A. Shatalov, and E. Wahba (2006), Numerical simulations of incompressible aerodynamic flows using viscous/inviscid interaction procedures, *Computer methods in applied mechanics and engineering*, *195*(23), 3110–3127.

Hafez, M., A. Shatalov, and M. Nakajima (2007), Improved numerical simulations of incompressible flows based on viscous/inviscid interaction procedures, *Computers & Fluids*, *36*(10), 1588–1591.

Iafrati, A., and E. Campana (2003), A domain decomposition approach to compute wave breaking (wave-breaking flows), *International journal for numerical methods in fluids*, *41*(4), 419–445.

Issa, R. I. (1986), Solution of the implicitly discretised fluid flow equations by operator-splitting, *Journal of computational physics*, *62*(1), 40–65.

Katz, J., and A. Plotkin (2001), *Low-speed aerodynamics*, vol. 13, Cambridge University Press.

Kim, K., A. I. Sirviente, and R. F. Beck (2005), The complementary rans equations for the simulation of viscous flows, *International journal for numerical methods in fluids*, *48*(2), 199–229.

Lighthill, M. (1958), On displacement thickness, *Journal of Fluid Mechanics*, *4*(4), 383–392.

Morino, L. (1986), Helmholtz decomposition revisited: vorticity generation and trailing edge condition, *Computational Mechanics*, *1*(1), 65–90.

Rempfer, D. (2006), On boundary conditions for incompressible navier-stokes problems, *Applied Mechanics Reviews*, *59*(3), 107–125.

Rosemurgy, W., D. Edmund, K. Maki, and R. Beck (2012), A velocity decomposition approach for steady free-surface flow, in *29th Symposium on naval hydrodynamics, Gothenburg, Sweden*.

Rosemurgy, W. J. (2014), A velocity decomposition approach for lifting and free-surface flow, Ph.D. thesis, The University of Michigan.

Rosemurgy, W. J., D. O. Edmund, K. J. Maki, and R. F. Beck (2011), A method for resistance prediction in the design environment, in *11th International Conference on Fast Sea Transportation FAST*.

Rosemurgy, W. J., K. J. Maki, and R. F. Beck (2013), The application of velocity decomposition to airfoil problems, in *28th International workshop on water waves and floating bodies, Marseille, France*.